Spectral Geometry of Vacuum Entanglement on Q_3 and Q_4: Gauge Couplings, the Gravitational Constant, the Vacuum Expectation Value, and the String Tension

Thomas A. Graham

July 24, 2026

Abstract

The vacuum is taken to be a network of entanglement bonds on a MERA over Q_3, each Planck-area bond a harmonic oscillator with relative entropy coordinate D_{KL}, bounded by the Bekenstein–Hawking value $\log\chi = S_{\mathrm{BH}}\ell_P^2/A = 1/4$, where χ is the effective bond dimension. The partition function gives vacuum entanglement $S^* = 2/9$ and residual $\xi^* = \log\chi - S^* = 1/36$. An eigenvalue scan of the MERA/Q_3 selects the central $17/16$, setting the model coupling $g^2(m_P) = 17/72$. Under the Q_3 1+2 split, z isometric and x, y disentanglers, $\mathrm{SU}(3)_c$ is assigned the matching bundle, $\mathrm{SU}(2)_L$ the xy-face loops, $\mathrm{U}(1)_Y$ the body diagonal. The matching bundle carries no closed contour, the strong coupling unmodified. On Q_3 the entanglement oscillator bond action is $M_{Q_3} = \kappa_P(I_{12} + c_I I_z - c_C C)$, carrying I_z the isometric incidence ($c_I = 4\xi^*$, the open star of the z-edge) and C the composite of the disentangler and isometry ($c_C = 2\xi^*$, the two diagonal placements per face). With PDG strong coupling as input, the bond action places the weak and hypercharge couplings within 0.10% and 0.056% of the PDG values, with $\sin^2\theta_W$ at 0.025% of PDG. Extending Q_3 along τ, the Euclidean time axis, gives the prism $Q_4 = Q_3 \times I$, whose residual entanglement edge weights $\omega_k = 1 + c_D\big(D_{xy}^{(Q_4)}\mathbf{1}\big)_k$ curve the geometry ($c_D = \frac{5}{\sqrt{2}}\xi^*$, the closed star per unit diagonal), closing $G_N = 0.999057\,\ell_P^2$ to 0.094%. From Q_4, the vertex operator's Higgs mode yields the vacuum expectation value $v = 246.9$ GeV (0.28%) and the edge operator's colour flux gives the string tension $\sqrt{\sigma} = 422.4$ MeV (0.44%, hadron spectrum).

Contents

1 Introduction

Several programs derive gauge or gravitational structure from quantum entanglement [1, 2, 3], or from the multi-scale entanglement renormalization ansatz (MERA) as discrete holographic geometry [4]. Other programs derive the Standard Model gauge group from a division algebra [5] or qubit entanglement [31]. Related programs obtain gauge and gravitational structure from a spectral principle. Connes' noncommutative geometry [6, 7] produces the gauge cluster and the Einstein–Hilbert action from the Dirac spectrum on the algebra $\mathbb{C} \oplus \mathbb{H} \oplus M_3(\mathbb{C})$, and, recently, during the preparation of this manuscript, Singh [8] derived the Standard Model coupled to Einstein–Weyl gravity from generalized trace dynamics on a noncommutative space of quaternions and octonions via the Dirac-operator spectral action.

The proposed model herein takes the Bekenstein–Hawking bound and the strong sector, both at the Planck scale, to be the foundational bridge between Planck-scale astrophysics and Planck-scale high-energy particle physics. The framework connects the two high-energy regimes by requiring both to share the same finite entanglement-capacity bound. Black-hole entropy supplies the maximum entanglement entropy, and the strong sector is the point of zero accumulated entanglement fluctuation, from which the proposed model is derived.

The vacuum is constructed as a network of entanglement bonds, one quantum harmonic oscillator on each Planck area of horizon, its coordinate the Umegaki relative entropy D_{KL}, saturating at the Bekenstein–Hawking bound [9, 10] $\log\chi = 1/4$. A binary MERA on the three-cube Q_3 follows, fixed by that saturation and the dimensionality of space, giving the gauge cluster on Q_3 and, through Sakharov's mechanism [11] on the prism $Q_4 = Q_3 \times I$ formed by extending the cube along τ, the Euclidean time axis, the gravitational constant. Both follow from one disentangler deformation of the bond action. The gravitational constant is derived from the complete propagator trace of the vertex operator. The vacuum expectation value is derived from a single mode of the vertex operator, the Higgs field, and the string tension is derived from the colour flux on the edge operator, these two carried from the Planck scale to the infrared by the descent. The residual capacity ξ^* sets the descent. It is the residual entanglement capacity below the Bekenstein–Hawking bound, $\xi^* = \log\chi - S^*$, processed per layer of the coarse-graining descent, its reciprocal $1/\xi^* = 36$ the depth of the descent.

2 Vacuum Entanglement

2.1 The bond coordinate

An elementary bond of the entanglement network is identified with one Planck area of horizon. The Bekenstein–Hawking area law [9, 10] $S = A/(4\ell_P^2)$ assigns each Planck area an entropy of $\frac{1}{4}$, fixing the maximum entanglement entropy carried by one bond at

$$\log\chi \;=\; \frac{S_{\mathrm{BH}}\,\ell_P^2}{A} \;=\; \tfrac{1}{4}. \tag{1}$$

The value $\log\chi = 1/4$ is the Bekenstein–Hawking area-law coefficient inherited through the bond–area identification, where χ is the effective bond dimension, accommodating the continuous, smooth geometric area law rather than forcing the entropy to scale in discrete, integer multiples.

The network consists of sites connected pairwise by bonds, each bond carrying entanglement capacity $\log\chi$. Each bond (i, j) carries a scalar coordinate, the Umegaki relative entropy [12]

$$D_{\mathrm{KL}}(\rho_{ij}\|\rho^0_{ij}) = \mathrm{tr}\big(\rho_{ij}\log\rho_{ij} - \rho_{ij}\log\rho^0_{ij}\big), \tag{2}$$

the reduced bond state ρ_{ij} measured against a reference ρ^0_{ij}. Two references enter and are not interchangeable. The structured MERA vacuum ρ^0_{ij} has non-flat spectrum and per-site von Neumann entropy S^* ($0 < S^* < \log\chi$), and $D_{\mathrm{KL}}(\rho_{ij}\|\rho^0_{ij})$ vanishes there. The maximally mixed reference σ^0_{ij} gives $D_{\mathrm{KL}}(\rho\|\sigma^0) = \log\chi - S(\rho)$, the capacity left below the bound and the reference of the static Bekenstein–Hawking normalisation. The dynamical bond coordinate is the relative entropy against the structured vacuum.

Within the Rényi family $D_\alpha(\rho\|\sigma) = \frac{1}{\alpha-1}\log\operatorname{tr}(\rho^\alpha\sigma^{1-\alpha})$, the coordinate (2) is the $\alpha\to 1$ member, recovered as the L'Hôpital limit $\lim_{\alpha\to 1} D_\alpha(\rho\|\sigma) = \operatorname{tr}[\rho(\log\rho - \log\sigma)]$. It is the unique member of that family satisfying all four of:

1. **Positive semi-definite:** $D_{\rm KL} \geq 0$, with equality iff $\rho_{ij} = \rho^0_{ij}$ (Klein's inequality).
2. **Thermodynamic:** $\delta D_{\rm KL} = \delta\langle K\rangle - \delta S$ with $K = -\log\rho^0$ the modular Hamiltonian (quantum first law of entanglement).
3. **Geometric:** $\delta D_{\rm KL} = \delta A_{\rm min}/4\ell_P^2$ (the linearised Ryu–Takayanagi first law [2]).
4. **Bounded:** $D_{\rm KL} \leq \log\chi$, the Bekenstein–Hawking bound.

The first law selects $\alpha = 1$, requiring $\operatorname{tr}[\rho\,\delta\log\rho] = 0$, ρ entering linearly under the trace after variation, which holds for $D_{\rm KL}$ at $\alpha = 1$ where $\delta D_{\rm KL} = \delta\langle K\rangle - \delta S$. The Ryu–Takayanagi bridge requires $K = -\log\sigma$ at $\alpha = 1$, and the Bekenstein–Hawking bound takes its scale from the static identity $D_1(\rho\|\sigma^0) = \log\chi - S(\rho)$ at $\alpha = 1$. The exclusion of the other Rényi members and the non-Rényi measures is given in Appendix A.

2.2 Harmonic oscillator

Each bond carries the quadratic potential $V_{ij} = \frac{1}{2}\kappa D_{\rm KL}^2$ in the coordinate (2). The framework places the bond at the Gaussian fixed point, at which the interaction couplings κ_n ($n \geq 3$) vanish. Therefore

$$\left.\frac{\partial^n V}{\partial D_{\rm KL}^n}\right|_{D_{\rm KL}=0} = 0 \qquad (n \geq 3), \tag{3}$$

and the bond potential is quadratic, $V = \frac{1}{2}\kappa D_{\rm KL}^2$.

2.3 Partition function and residual vacuum entanglement

The bond coordinate $D_{\rm KL}(\rho\|\rho^0)$ of §2.1 is a relative entanglement entropy. Its trace, $\operatorname{tr}(\rho\log\rho - \rho\log\rho^0)$, is taken inside the coordinate, and what it returns is a real number. It is the entanglement accumulated on that bond above the structured vacuum. It is the coordinate of the bond oscillator of §2.2 and the field ϕ_e integrated over in the bond action of §3.3. The partition function of one RG step is therefore a classical sum over the bond configurations of the layer, weighted by the total bond coordinate. A layer has N input sites and one output site,

$$Z_{N+1}(\beta) \;=\; \sum_{\{\rho_i\}} \exp\Big(-\beta\sum_{i=1}^{N+1} D_{\rm KL}(\rho_i\|\rho_i^0)\Big), \tag{4}$$

the sum running over the configurations accessible to the $N+1$ sites.

With $F = -\beta^{-1}\log Z$ and $\big\langle\sum_i D_{\rm KL}(\rho_i\|\rho_i^0)\big\rangle = -\partial_\beta\log Z$, the thermodynamic entropy is

$$S \;=\; \beta^2\frac{\partial F}{\partial\beta} \;=\; \big(1-\beta\,\partial_\beta\big)\log Z \;=\; \log Z + \beta\,\Big\langle\sum_{i=1}^{N+1} D_{\rm KL}(\rho_i\|\rho_i^0)\Big\rangle. \tag{5}$$

At the structured vacuum every site sits at its reference, $\rho_i = \rho_i^0$, so $D_{\rm KL}(\rho_i\|\rho_i^0) = 0$ by Klein's inequality, the exponent of (4) vanishes identically, and with it the expectation in (5). The parameter β multiplies that expectation, so $S_{\rm layer} = \log Z|_{\rm vac}$ at every β.

Each site carries entanglement entropy bounded by the Bekenstein–Hawking capacity $\log\chi$ of §2.1, and the free layer saturates it. The coarse-graining map is the adjoint $w^\dagger$ of the isometry $w:\mathscr{H}\to\mathscr{H}^{\otimes N}$, $w^\dagger w = \mathbb{I}$, and the output is a deterministic function of the inputs, $S(\text{output}\mid i_1,\ldots,i_N) = 0$, so the entropy of the layer is carried by the N input sites,

$$\log Z_{\rm free} \;=\; \sum_{i=1}^{N+1}\log\chi \;=\; (N+1)\log\chi \tag{6}$$

$$S_{\rm layer} \;=\; \log Z\Big|_{\rm vac} \;=\; (N+1)\log\chi - \log\chi \;=\; N\log\chi. \tag{7}$$

With $d = 3$ the cell of one layer is the three-cube Q_3: its 8 vertices are the input sites and its centre is the output site, so $N = 8$ and $N+1 = 9$. The B_3 symmetry of Q_3 acts transitively on the 8 vertices, so the input sites carry equal entanglement. The layer comprises these 8 vertices together with the output site at the centre, and S^* is the entropy per site of the layer, averaged over all $N+1$ of its sites. With $\log\chi = \frac{1}{4}$ from the Bekenstein–Hawking bound of §2.1,

$$S_{\text{layer}} \;=\; N\log\chi \;=\; 8\cdot\tfrac{1}{4} \;=\; 2 \tag{8}$$

$$S^* \;=\; \frac{S_{\text{layer}}}{N+1} \;=\; \frac{N\log\chi}{N+1} \;=\; \frac{2}{9} \tag{9}$$

$$\xi^* \;=\; D_{\text{KL}}(\rho^0\|\sigma^0) \;=\; \log\chi - S^* \;=\; \frac{1}{4}-\frac{2}{9} \;=\; \frac{1}{36} \tag{10}$$

The residual ξ^* is itself a relative entanglement entropy, the residual vacuum entanglement entropy, the bond coordinate of the structured vacuum ρ^0 measured against the flat reference σ^0 of §2.1, which satisfies $D_{\text{KL}}(\rho\|\sigma^0) = \log\chi - S(\rho)$. It is the residual capacity, the entanglement the vacuum leaves below the bound. Substituting S^* of (9) into $\xi^* = \log\chi - S^*$ gives the general-N form,

$$\xi^* \;=\; \log\chi - \frac{N\log\chi}{N+1} \;=\; \frac{(N+1)\log\chi - N\log\chi}{N+1} \;=\; \frac{\log\chi}{N+1}. \tag{11}$$

2.4 Eigenvalue scan and selection of MERA

The multi-scale entanglement renormalization ansatz (MERA) is a network of bonds. Each layer takes the N input sites of the unit cell, factors out their short-range entanglement via disentanglers on the bonds, then coarse-grains isometrically ($w^\dagger w = \mathbb{I}$) to one output site. The branching factor b is the linear scale of the coarse-graining and n the cell's spatial dimension, so a MERA on the n-cube Q_n has $N = b^n$ input sites. With $b = 2$ (binary MERA) and $n = 3$ (observed spatial dimension), the cell is Q_3 with $N = 2^3 = 8$ vertices. The disentangling step at each layer is proposed to generate the gauge fields of that scale on the cell edges. This binary MERA on Q_3 is selected below through an eigenvalue scan across candidate tensor-network structures on the cube.

The MERA spectrum. On the three-cube, vertices ordered $000, 001, 010, 011, 100, 101, 110, 111$ by $v = 4x+2y+z$ and two vertices joined when their coordinates differ in one bit, the entanglement matrix is

$$M_{\text{ent}} \;=\; \mathbb{I} + (\log\chi)^2 A(Q_3), \tag{12}$$

with $A(Q_3)$ the cube adjacency and $(\log\chi)^2 = 1/16$. Its spectrum, $\lambda = 1+(\log\chi)^2\mu$ for $\mu\in\{3,1,-1,-3\}$, is

$$\text{Spec}(M_{\text{ent}}) \;=\; \left\{\, \tfrac{19}{16}^{(1)},\ \tfrac{17}{16}^{(3)},\ \tfrac{15}{16}^{(3)},\ \tfrac{13}{16}^{(1)} \,\right\}, \tag{13}$$

the multiplicities $\binom{3}{0},\binom{3}{1},\binom{3}{2},\binom{3}{3}$ the binomial signature of Q_3. The central eigenvalue $17/16 = 1+(\log\chi)^2$ at multiplicity 3 is the $\mu = +1$ mode with the entanglement scale $(\log\chi)^2 = 1/16$.

Multiplied by the vacuum entanglement $S^* = 2/9$, the four eigenvalues give four candidate couplings $S^*\lambda$. Against the PDG strong coupling $g_s^2(m_P) = 0.237350$, only the central $17/72$ lies near the measured value. The neighbours miss by more than eleven percent. The strong coupling selects the central eigenvalue of the spectrum, and the model runs on this $17/72$.

The ratio. With $S^* = 2/9$ from the partition function on the cube at the Bekenstein–Hawking bound, and $g_s^2(m_P) = 0.237350$ the PDG value at the Planck scale, the ratio is

$$\frac{g_s^2(m_P)}{S^*} \;=\; \frac{0.237350}{2/9} \;\approx\; \frac{0.236111}{2/9} \;=\; \frac{17/72}{2/9} \;=\; \mathbf{\frac{17}{16}} \;=\; 1+(\log\chi)^2, \tag{14}$$

setting the model set value $g^2(m_P) = 17/72 = 0.236111$ (-0.52% residual against PDG $g_s^2(m_P)$).

eigenvalue λ	mult.	$S^*\lambda$	value	residual vs $g_s^2(m_P)$
$19/16$	1	$19/72$	0.263889	$+11\%$
$\mathbf{17/16}$	3	$\mathbf{17/72}$	**0.236111**	$\mathbf{-0.52\%}$
$15/16$	3	$5/24$	0.208333	-12%
$13/16$	1	$13/72$	0.180556	-24%

Table 1: The four eigenvalues of M_{ent} times the vacuum entanglement $S^* = 2/9$. Only the central $17/72$ lies near the PDG strong coupling $g_s^2(m_P) = 0.237350$, the neighbours missing by over eleven percent.

MERA spectrum and gauge. Multiplying through by S^*:

$$\langle D_{\text{KL}} \rangle_\square \;=\; S^*\left[1 + (\log\chi)^2\right] \;=\; \frac{2}{9}\cdot\frac{17}{16} \;=\; \frac{17}{72}. \tag{15}$$

$\langle D_{\text{KL}} \rangle_\square$ is the plaquette-averaged entanglement, the relative-entropy deformation of the bond density matrices from the maximally mixed reference, averaged over the four edges of a square face of Q_3 at the BH-saturated fixed point. The value $17/72$ is the model. It approximates the physical $g_s^2(m_P)$ to 0.52% (Table 5).

Selection of binary MERA on Q_3. This spectrum is that of a binary MERA ($b = 2$) on the $n = 3$ cube, with $N = b^n = 8$. The central eigenvalue $17/16$ at multiplicity 3 reproduces the ratio derived above, and the degeneracy pattern $\{1, 3, 3, 1\}$ is the binomial signature of Q_3. The simultaneous conditions for this cell are shown in Table 2, and condition by condition for the binary row in Table 3.

$b \setminus n$	$n = 1$	$n = 2$	$n = 3$	$n = 4$	$n \geq 5$
$b = 2$	$\times$	$\times$	✓	$\times$	$\times$
$b = 3$	$\times$	$\times$	$\times$	$\times$	$\times$
$b = 4$	$\times$	$\times$	$\times$	$\times$	$\times$
$b \geq 5$	$\times$	$\times$	$\times$	$\times$	$\times$

Table 2: (b,n) parameter scan, pass/fail of the simultaneous conditions (i)–(iv) for b-ary MERA on the cell $\{0,\ldots,b-1\}^n$. The unique cell is $(b,n) = (2,3)$. Failures at $b \geq 3$ for $n \geq 3$ arise from BH-bond-capacity overshoot ($N = b^n$ exceeds the $\log\chi = 1/4$ bound); failures at $n \neq 3$ for $b = 2$ arise as shown in Table 3.

	Condition	$n = 1$ ($N = 2$)	$n = 2$ ($N = 4$)	$n = 3$ ($N = 8$)	$n = 4$ ($N = 16$)
(i)	$d_{\text{spacetime}} = n + 1 = 4$	no	no	yes	no
(ii)	$(\log\chi)^2 = 1/(2N)$ at $\log\chi = 1/4$	no	no	yes	no
(iii)	eigenvalue $17/16$ of $\mathbb{I} + \log\chi^2 A$ at mult n	yes	no	yes	no
(iv)	1+2 split with ≥ 1 disentangler axis	no	yes	yes	yes

Table 3: Status of conditions for binary MERA ($b = 2$) in n spatial dimensions. Conditions (i) and (ii) each independently select $n = 3$. The remaining conditions corroborate. The spectral condition (iii) shows $n = 2$ and $n = 4$ lack the central-identity eigenvalue $17/16$; the 1+2 split condition (iv) excludes the disentangler-free $n = 1$ cell. Condition (iii) also holds at $n = 1$, since $17/16$ occurs for every odd n, so it is corroborative, not selective. The pairing of condition (ii) and the 1+2 split of condition (iv) are developed in §2.5.

2.5 The 1+2 anisotropic split

The selection of binary MERA on Q_3 in §2.4 gives a structural split of the 12 edges of Q_3 into an isometric bundle and a disentangler bundle.

Disentanglers and isometries in MERA. The MERA construction [15, 16, 4] alternates two operations: *disentanglers* $u : V \otimes V \to V \otimes V$, unitaries acting on pairs of adjacent sites to remove short-range entanglement; and *isometries* $w : V \to V^{\otimes b^n}$, whose adjoints $w^\dagger$ are the coarse-graining maps that take b^n input sites to one output site. Two structural features follow:

- Disentanglers are two-site unitaries. In the xy coarse-graining plane they sit on the *diagonals* of each xy-face, the two opposite corners of the square, not on single vertices, since one vertex carries a single site and cannot carry a two-site unitary. Their action reaches the bond field on the four edges of that face through the in-plane operator D_{xy} of §4.
- Isometries act in the *coarse-graining direction*. For branching factor $b = 2$ there is one such direction; the remaining $n-1 = 2$ directions are within-layer, on which the disentanglers act.

With $(b,n) = (2,3)$ selected in §2.4, one axis of Q_3 is the isometric coarse-graining axis and the other two axes carry disentanglers. The disentanglers sit on the diagonals of the two xy-faces, the opposite-corner pairs at $z = 0$ and $z = 1$. These diagonals are not edges of Q_3 and carry no bond field ϕ_e of their own; the disentangler's effect reaches the bond field on the edges through the operator D_{xy}.

Edge partition. Let a count axes of Q_3 carrying isometric bonds and b count axes carrying disentangler bonds, with $a + b = 3$ (every axis carries one role; each direction contains 4 parallel edges of Q_3). The four possibilities are:

- $a = 3, b = 0$ (all-isometric): no disentanglers means no bond-level entanglement structure, giving a tree tensor network with $D_{\mathrm{KL}} \equiv 0$ and contradicting $S^* = 2/9$.
- $a = 2, b = 1$ (two-isometric, one-disentangler): two coarse-graining directions carry a 2D RG flow parameter, not the single coarse-graining scale of a binary MERA.
- $a = 0, b = 3$ (no-isometric): no coarse-graining direction; not a MERA.
- $a = 1, b = 2$ (one-isometric, two-disentangler): 4 edges parallel to the isometric axis form the isometry bundle; the 8 edges in the perpendicular plane form the disentangler bundle.

Only $a = 1, b = 2$ is consistent with binary MERA on Q_3. This is the 1+2 split.

Axis labeling. The B_3 symmetry of Q_3 allows any of the three coordinate axes to play the isometric role. Naming the isometric axis z, the B_3 subgroup $\sigma_{xy} : (\xi_1, \xi_2, \xi_3) \mapsto (\xi_2, \xi_1, \xi_3)$ fixes z and permutes the other two axes. σ_{xy} is the surviving symmetry of the disentangler bundle (it swaps the x- and y-direction edges while preserving the bundle setwise). The choice of z as the isometric axis is a labeling convention; observables are invariant under the three axis relabelings.

Matching and disentangler bundles. With z as the isometric axis:

- The *matching bundle* E_z is the set of 4 edges of Q_3 parallel to z. Each z-edge runs from one $z = 0$ vertex to one $z = 1$ vertex; the four z-edges together cover all 8 vertices of Q_3 once.
- The *disentangler bundle* E_{xy} is the set of 8 edges of Q_3 parallel to x or y. These are the boundary edges of the two xy-faces ($z = 0$ and $z = 1$), 4 edges around each face. The induced subgraph G_{xy} has degree 2 at every vertex, and σ_{xy} acts on it as the axis swap $x \leftrightarrow y$.

Bundle decomposition of the central identity. The residual capacity $\xi^* = \log\chi - S^* = 1/36$ of (10) is the room per bond above the per-site vacuum entanglement. The central identity $\langle D_{\mathrm{KL}}\rangle_\square = S^*(1+(\log\chi)^2) = 17/72$ of §2.4 decomposes across the two bundles as follows.

On E_z, the isometry constraint $w^\dagger w = \mathbb{I}$ preserves the full per-site vacuum entanglement. The output state is a pure function of the inputs and the isometry contributes no entropy beyond what the input bonds already carry. The per z-bond entanglement is therefore

$$\langle D_{\mathrm{KL}}\rangle_z \;=\; S^* \;=\; \tfrac{2}{9}. \tag{16}$$

On E_{xy}, the per-bond entanglement follows two independent routes. The first reads it from the entanglement matrix $M_{\mathrm{ent}} = I + (\log\chi)^2 A(Q_3)$ of §2.4, whose central eigenvalue $1+(\log\chi)^2 = 17/16$ gave the identity. The disentangler piece is the $(\log\chi)^2$ term of that eigenvalue weighted by S^*,

$$\langle D_{\mathrm{KL}}\rangle_{xy} \;=\; (\log\chi)^2 S^* \;=\; \tfrac{1}{16}\cdot\tfrac{2}{9} \;=\; \tfrac{1}{72}. \tag{17}$$

The second reads it from the disentangler bundle directly. The residual capacity per site is ξ^*, and the induced subgraph G_{xy} has degree 2. Each vertex meets two disentangler edges. At the scale-invariant fixed point the state is invariant under σ_{xy}, the $x \leftrightarrow y$ swap that is the symmetry of E_{xy}, so the two disentangler directions carry equal weight and the per-site residual ξ^* is shared equally between the two incident edges, half to each,

$$\langle D_{\mathrm{KL}}\rangle_{xy} \;=\; \frac{\xi^*}{2} \;=\; \frac{1}{2}\cdot\tfrac{1}{36} \;=\; \tfrac{1}{72}. \tag{18}$$

The pairing (condition ii). The two routes (17) and (18) are independent. The first uses the eigenvalue of M_{ent}, the second the residual ξ^* and the σ_{xy} equipartition. They are different functions of N and $\log\chi$, and requiring them to agree is a self-consistency of the scale-invariant fixed point. Equating them, $(\log\chi)^2 S^* = \xi^*/2$, and substituting the partition-function values $S^* = N\log\chi/(N+1)$ and $\xi^* = \log\chi/(N+1)$ of (9) and (11),

$$(\log\chi)^2 S^* \;=\; \frac{\xi^*}{2} \qquad\Longrightarrow\qquad (\log\chi)^2\,\frac{N\log\chi}{N+1} \;=\; \frac{1}{2}\,\frac{\log\chi}{N+1}. \tag{19}$$

Both sides carry the factor $\log\chi/(N+1)$; multiplying through by $(N+1)/\log\chi$,

$$(\log\chi)^2 N \;=\; \frac{1}{2} \qquad\Longrightarrow\qquad (\log\chi)^2 \;=\; \frac{1}{2N}, \tag{20}$$

condition (ii) of Table 3. The two routes are not equal for general N; they coincide only on this relation, so the agreement is a constraint, not an identity. At $\log\chi = 1/4$ and $N = 2^3 = 8$,

$$\left(\tfrac{1}{4}\right)^2 \;=\; \frac{1}{16} \;=\; \frac{1}{2\cdot 8}. \tag{21}$$

Summing the two bundle contributions reproduces the central identity:

$$\langle D_{\mathrm{KL}}\rangle_\square \;=\; \langle D_{\mathrm{KL}}\rangle_z + \langle D_{\mathrm{KL}}\rangle_{xy} \;=\; S^* + (\log\chi)^2 S^* \;=\; S^*\bigl(1+(\log\chi)^2\bigr) \;=\; \tfrac{17}{72}. \tag{22}$$

The 1+2 split labels the two terms of the central eigenvalue $17/16 = 1+(\log\chi)^2$: the "1" is the isometric contribution carried by E_z, and the "$(\log\chi)^2$" is the disentangler contribution carried by E_{xy}.

The prism Q_4 extends the cube by one isometric MERA step, the split carrying over with a temporal direction τ, the Euclidean time axis, joining the in-plane axes x, y and the isometric axis z, the substrate for emergent gravity of §8.

3 Gauge Structure

3.1 Gauge sectors on the cube

The 1+2 split of §2.5 partitions the twelve edges of Q_3 into two bundles, the matching bundle E_z, the four edges parallel to the isometric z-axis, and the disentangler bundle E_{xy}, the eight edges parallel to x or y (the boundary edges of the two xy-faces at $z = 0$ and $z = 1$). A third substrate is the body diagonal, the open line from (000) to (111) joining the two antipodal corners through the cube. The three Standard-Model factors are carried by Wilson observables (§3.3) on these substrates, a closed loop on a face, a closed contour on the matching bundle, and an open line on the body diagonal.

Two observable types, closed and open. The Wilson contour C is the signed bond-field sum $\sum_{e\in C} b_e \phi_e$ (§3.3). A *closed* contour ($\partial_1 b = 0$) measures the gauge-invariant flux through the surface it bounds. An *open* contour is sourced at its two endpoints, where the external charges sit. The abelian factor is the open line, the two non-abelian factors the two closed substrates.

U$(1)_Y$: the body diagonal. The abelian factor is the body-diagonal line. It crosses all three axes once and joins the antipodal vertices (000) and (111). Under the residual disentangler symmetry σ_{xy} : $(\xi_1, \xi_2, \xi_3) \mapsto (\xi_2, \xi_1, \xi_3)$ of §2.5, which swaps the x- and y-axes and fixes z, both endpoints (000) and (111) are fixed, so the body diagonal is σ_{xy}-invariant. It passes through the centre of the cube; in the edge basis it is represented by the staircase $(000) \to (100) \to (110) \to (111)$, three edges one along each axis, carrying the circumradius weight $\sqrt{3}/2$ of the through-centre diagonal.

SU$(2)_L$: the face loops. The first non-abelian factor is the closed 4-cycle bounding an xy-face. All four edges of such a face lie in the disentangler bundle E_{xy}, so the weak loop is supported entirely on the disentangler plane. The face is a nontrivial closed cycle enclosing flux, so the weak loop carries a nonzero correction, $\delta_L \neq 0$ (§3.5). Under σ_{xy} the two horizontal xy-faces ($z = 0$ and $z = 1$) are fixed and the four vertical faces are paired, so the substrate sits in the plane the disentanglers act on. The two xy-faces give the same Wilson exponent.

SU$(3)_c$: the matching bundle. The second non-abelian factor is the matching bundle E_z, the isometry direction of the split. The four z-edges meet each of the eight vertices of Q_3 once, so the only closed contour supported on E_z is the trivial one; the strong observable therefore carries no correction from the bond action, $\delta_s = 0$ (§3.4). Under coarse-graining, the adjoint map $w^\dagger$ carries E_z to the matching bundle of the next layer, so the colour substrate is an invariant subspace at every scale. Under σ_{xy} the z-edges map to z-edges: E_z is fixed setwise, with its in-plane endpoint labels $x \leftrightarrow y$ permuted. The colour multiplicity is $N_c = 3$.

The resulting gauge cluster is

$$SU(3)_c \times SU(2)_L \times U(1)_Y, \qquad \text{colour multiplicity } N_c = 3, \tag{23}$$

with substrate and σ_{xy} action per factor in Table 4.

Sector	Substrate	σ_{xy} action on substrate
$SU(3)_c$	matching bundle E_z (the four z-edges)	fixes E_z setwise; permutes the $x \leftrightarrow y$ endpoint labels
$SU(2)_L$	4-cycle bounding an xy-face	fixes the two horizontal faces, pairs the four vertical faces
$U(1)_Y$	body diagonal $(000) \to (111)$	fixes both endpoints; the body diagonal is invariant

Table 4: Sector substrate and gauge-factor identification on Q_3. The σ_{xy} column is the action of the disentangler symmetry on each substrate.

The assignment is kinematic. The substrates and their σ_{xy} action follow from the geometry of Q_3 and the 1+2 split of §2.5. No fixed point, continuum limit, or renormalization-group flow enters.

3.2 Plaquette identification: $\langle(\Omega^a_\Box)^2\rangle = \langle D_{\mathrm{KL}}\rangle_\Box$

At the Planck scale, two distinct structures coincide on every plaquette of Q_3. Bekenstein–Hawking bond saturation (D_{KL} approaching $\log\chi = 1/4$ from the BH bound) and Wilson lattice matching at lattice spacing $a = \ell_P$. Both govern per-plaquette quadratic fluctuations at the same scale.

Wilson side: $\langle(\Omega^a_\Box)^2\rangle = g^2$. The Wilson lattice action [18, 19] with link variables $U_{ij} = \exp(i\xi^a_{ij}T^a) \in \mathrm{SU}(N_c)$ and $\mathrm{tr}(T^aT^b) = \delta^{ab}/2$ is

$$S_W = \frac{2N_c}{g^2}\sum_\Box\left(1 - \tfrac{1}{N_c}\mathrm{Re}\,\mathrm{Tr}\,U_\Box\right). \tag{24}$$

Expanding $U_\Box = \exp(i\Omega^a_\Box T^a)$, the quadratic part of the plaquette is

$$1 - \tfrac{1}{N_c}\mathrm{Re}\,\mathrm{Tr}\,U_\Box \;\longrightarrow\; \frac{\Omega^2_\Box}{4N_c}, \tag{25}$$

using $\mathrm{tr}[(T^a)^2]/N_c = 1/(2N_c)$, which fixes the coupling normalisation

$$S_W = \frac{1}{2g^2}\sum_\Box \Omega^2_\Box. \tag{26}$$

At the Gaussian fixed point the entanglement action carries no vertices beyond the quadratic, so this is the bond action in the flux variables, and the vacuum measure e^{-S_W} is Gaussian in the N_c^2-1 adjoint components $\Omega^a_\Box$ with variance set by the action coefficient. For each adjoint component independently,

$$\langle\Omega^a_\Box\Omega^b_\Box\rangle = g^2\,\delta^{ab}, \tag{27}$$

so the plaquette flux per adjoint component, averaged in the vacuum, is $\langle(\Omega^a_\Box)^2\rangle = g^2$.

Entanglement side: $\langle D_{\mathrm{KL}}\rangle_\Box = S^*(1+\log\chi^2)$. The central identity (15) derived in §2.4 gives

$$\langle D_{\mathrm{KL}}\rangle_\Box = S^*\left(1+\log\chi^2\right) = g^2(m_P), \tag{28}$$

the plaquette-averaged entanglement at the BH-saturated fixed point on Q_3.

Plaquette identification. Both sides of the plaquette identification measure the per-plaquette deformation from the symmetric reference. $\langle D_{\mathrm{KL}}\rangle_\Box$ measures the deviation of the bond density matrices from the maximally mixed reference σ^0. By definition $D_{\mathrm{KL}}(\rho\|\sigma^0) = 0$ iff $\rho = \sigma^0$, with $D_{\mathrm{KL}}(\rho\|\sigma^0) \geq 0$ otherwise. $\langle(\Omega^a_\Box)^2\rangle$ measures the deviation of the Wilson holonomy from the identity. The Wilson plaquette action is $\propto (1 - \frac{1}{N_c}\mathrm{Re}\,\mathrm{Tr}\,U_\Box)$, which vanishes iff $U_\Box = \mathbb{I}$ and is positive otherwise. The bond-averaged entanglement is taken equal to the Wilson plaquette flux per adjoint component at the vacuum,

$$\langle D_{\mathrm{KL}}\rangle_\Box = \langle(\Omega^a_\Box)^2\rangle, \tag{29}$$

The plaquette identification (29) therefore sets $g^2(m_P) = S^*\left(1+\log\chi^2\right) = 17/72$. The Wilson side matches the central identity (15) of §2.4 through the plaquette identification.

3.3 The entanglement oscillator bond action on Q_3 and the Wilson contour

The plaquette identification of §3.2 sets the unmodified coupling at m_P as $g^2 = \langle D_{\mathrm{KL}}\rangle_\Box = g^2(m_P)$. This subsection sets up the quadratic action for the bond field on Q_3, from which the sector-specific corrections taking this unmodified value to (g_s^2, g_L^2, g_Y^2) at m_P are computed in §§3.4–3.6.

The bond field. On each of the $|E| = 12$ oriented edges $e \in E(Q_3)$, the bond field is the entropic coordinate

$$\phi_e \;:=\; D_{\mathrm{KL}}\big(\rho_e \,\big\|\, \rho_e^0\big), \tag{30}$$

where ρ_e is the bond density matrix and ρ_e^0 is the MERA fixed-point reference state on e. The joint configuration is the 12-vector $\phi = (\phi_{e_1}, \ldots, \phi_{e_{12}})$.

The entanglement oscillator bond action. The entanglement oscillator bond action is quadratic,

$$S[\phi] \;=\; \tfrac{1}{2}\,\phi^T M\,\phi, \qquad M \in \mathbb{R}^{12\times 12}, \tag{31}$$

with M a real symmetric positive-definite matrix indexed by the edges of Q_3. Its inverse is the bond–bond covariance, $(M^{-1})_{ee'} = \langle \delta\phi_e\,\delta\phi_{e'}\rangle$. This M is the bond-level counterpart of the vertex entanglement matrix M_{ent} of §2.4; its structure is derived below from the per-bond quadratic-potential expansion and the MERA mechanism decomposition.

***M* from the per-bond quadratic potential.** The per-bond expansion of D_{KL} (§2.2) gives the quadratic potential

$$V_e(\phi_e) \;=\; \tfrac{1}{2}\,\kappa_P\,\phi_e^2, \qquad \kappa_P \;=\; \frac{2}{(\log\chi)^2} \;=\; 32, \tag{32}$$

with the Bekenstein–Hawking saturation condition $V_{\max} = \frac{1}{2}\kappa_P(\log\chi)^2 = m_P$ fixing κ_P. This pins the diagonal $M_{ee} = \kappa_P$ for every edge. κ_P is the on-site coefficient of the bond oscillator (§2.2).

The off-diagonal entries of M are the cross-bond coefficients between bond oscillators, fixed by the cross-bond correlations generated by the MERA mechanisms of the 1+2 split, the isometry w along the privileged axis and the disentangler u transverse to it. The relevant class is the share-vertex mechanism, which correlates bonds meeting at a common vertex of Q_3 through the disentangler and isometry acting at that vertex. The mechanism and its contribution to M are derived in §4. Throughout §§3.4–3.6 below, the bare diagonal pinning is $M = \kappa_P I_{12}$; the off-diagonal corrections to δ_L and δ_Y then enter via M^{-1} in §4.

The contour phase of the bond entanglement. For any oriented contour $C \subset E(Q_3)$, a closed cycle (loop) or an open path (line), let $b \in \{0, \pm 1\}^{12}$ be its incidence vector. $b_e = +1$ if C traverses e in its positive orientation, -1 in the negative, 0 if $e \notin C$. Because ϕ_e is the entanglement (the relative entropy) on edge e, the sum $\sum_{e\in C} b_e\,\phi_e = b^T\phi$ is the oriented total of the bond entanglements along C, the entanglement accumulated around the contour. The phase carrying it is

$$W_C \;:=\; \exp\Big(i\textstyle\sum_{e\in C} b_e\,\phi_e\Big) \;=\; \exp(i\,b^T\phi). \tag{33}$$

Its expectation under the Gaussian bond measure (31) is the Gaussian integral $\langle e^{i b^T\phi}\rangle = e^{-\frac{1}{2}b^T M^{-1} b}$,

$$\langle W_C\rangle \;=\; \exp\Big(-\tfrac{1}{2}\,b^T M^{-1} b\Big), \tag{34}$$

so $b^T M^{-1} b$ is the variance of the accumulated entanglement around C, with M^{-1} the covariance of the bond entropies. Under the plaquette identification of §3.2 ($\langle D_{\mathrm{KL}}\rangle_\square = \langle(\Omega^a_\square)^2\rangle$), this phase is the Wilson contour. The quadratic action carries no vertices beyond M, so the exponent receives no further corrections. The coupling offset is therefore a second moment of the bond measure, the quadratic form $\frac{1}{2}\,b^T M^{-1} b$, and no higher cumulant of the flux enters its extraction; the Wilson form of §3.2 fixes the coupling normalisation, not the observable evaluated.

Sector-mapped Wilson correction. For a sector $G \in \{\mathrm{SU}(3)_c, \mathrm{SU}(2)_L, \mathrm{U}(1)_Y\}$, the canonical incidence vector b_G is the one given by the sector assignment of §3.1: the matching-bundle subspace for $\mathrm{SU}(3)_c$, a face 4-cycle for $\mathrm{SU}(2)_L$, a body-diagonal staircase for $\mathrm{U}(1)_Y$. The Wilson correction is

$$\delta_G \;:=\; -\log\langle W_{C_G}\rangle \;=\; \tfrac{1}{2}\, b_G^T M^{-1}\, b_G. \tag{35}$$

Equivalently, δ_G is the fluctuation of the entanglement accumulated around the sector contour C_G.

Deformation-function extension. At the plaquette level (§3.2), $\langle D_{\mathrm{KL}}\rangle_\square$ is the per-plaquette deformation function, equal to $\langle(\Omega^a_\square)^2\rangle$ of the Wilson lattice action. It is proposed that the deformation-function role of $\langle D_{\mathrm{KL}}\rangle$ extends from plaquettes to all canonical contours b_G. $\delta_G = \frac{1}{2}\, b_G^T M^{-1} b_G$ is the per-contour deformation analogous to $\langle(\Omega^a_C)^2\rangle$, and the disentangler's contribution to M propagates to all sector observables via M^{-1}.

Recurrent and transient sector formulas. The sector coupling $g_G^2(m_P)$ follows from the unmodified $g^2 = g^2(m_P)$ and δ_G via a formula whose form is given by the geometry of the canonical contour:

- **Wilson loop (face), recurrent.** A Wilson loop closes on itself; multiple traversals contribute, summing the geometric series $1+\delta+\delta^2+\cdots = (1-\delta)^{-1}$:

$$g_L^2(m_P) \;=\; \frac{g^2(m_P)}{1-\delta_L} \;=\; \frac{g_s^2(m_P)}{1-\delta_L}. \tag{36}$$

- **Wilson line (body diagonal), transient.** The body diagonal connects (000) to (111) and does not close; no multiple traversal exists, no geometric series arises, and the correction enters once at amplitude level:

$$g_Y^2(m_P) \;=\; g^2(m_P)\,(1-\delta_Y) \;=\; g_s^2(m_P)\,(1-\delta_Y). \tag{37}$$

With (35), (36), (37), the three sector predictions are closed forms in S^*, $\log\chi$, and the canonical contour lengths $|b_G|^2$. The sector observables b_G and their bare Wilson exponents (with the diagonal pinning $M = \kappa_P I_{12}$ alone) are set up sector-by-sector in §§3.4–3.6. The off-diagonal disentangler corrections to δ_L and δ_Y, and the resulting final $g_L^2(m_P)$ and $g_Y^2(m_P)$, are derived in §4.

3.4 Strong coupling

The $\mathrm{SU}(3)_c$ sector lives on the matching bundle E_z, the four z-edges of Q_3 that form the isometric coarse-graining direction of the 1+2 split (§2.5), oriented from each $z=0$ endpoint to its $z=1$ endpoint and listed in Appendix B. The four z-edges meet all eight vertices of Q_3 once. E_z, as a one-dimensional subcomplex, contains no cycle.

The closed-contour condition. Let $\partial_1 : C_1(Q_3) \to C_0(Q_3)$ be the oriented vertex–edge boundary map. For an edge e directed $u \to w$, $\partial_1 e = w - u$. For a contour $b = \sum_e b_e\, e$, with b_e its component on edge e, the *net flow* at a vertex x is $(\partial_1 b)_x$, the signed sum of the components on the edges meeting x. A Wilson contour is *closed* when its net flow vanishes at every vertex,

$$\partial_1 b = 0. \tag{38}$$

The strong Wilson correction (35) is $\delta_s = \frac{1}{2}\, b_s^\top M^{-1} b_s$. The incidence vector b_s is the strong contour, the Wilson contour of §3.3 carrying the $\mathrm{SU}(3)_c$ flux, supported on the colour substrate E_z and required by (38) to be closed.

The strong contour vanishes. Supported on E_z, the strong contour is the sum

$$b_s = c_1 e_0 + c_2 e_5 + c_3 e_8 + c_4 e_{11}, \tag{39}$$

where c_i is the component of b_s on the i-th z-edge of $E_z = \{e_0, e_5, e_8, e_{11}\}$, the signed weight with which the contour runs along that edge, and the four coefficients are fixed by the closure condition (38). Restricted to E_z, the boundary map is the 8×4 incidence matrix $B_z = \partial_1\big|_{E_z} \in \{-1, 0, +1\}^{8\times 4}$ (Appendix B). Because every vertex of Q_3 lies on one z-edge, each row of B_z carries a single nonzero entry, and the closure condition $B_z c = 0$ reduces to one one-term equation per vertex, $c_i = 0$ (Appendix B). Hence $c_1 = c_2 = c_3 = c_4 = 0$, and

$$b_s = c_1 e_0 + c_2 e_5 + c_3 e_8 + c_4 e_{11} = 0. \tag{40}$$

The coupling. With $b_s = 0$ from (40), the strong Wilson correction vanishes identically,

$$\delta_s = \tfrac{1}{2} b_s^\top M^{-1} b_s = \tfrac{1}{2} 0^\top M^{-1} 0 = 0, \tag{41}$$

for any positive-definite M. The off-diagonal structure of M does not enter, because M^{-1} acts on the zero vector. There is no strong Wilson contour. The recurrent formula (36) with $\delta_s = 0$ then sets the strong coupling equal to the unmodified coupling at the Planck scale,

$$g_s^2(m_P) = \frac{g^2(m_P)}{1-0} = g^2(m_P). \tag{42}$$

The strong coupling is taken to be the unmodified coupling itself. It is the sector against which the scan's eigenvalue selection was performed, and its residual is a result of model selection. With $\delta_s = 0$, the residual is the gap between it and measurement, and carries no contribution from M.

3.5 Weak coupling

The $\mathrm{SU}(2)_L$ sector is parameterised by Wilson loops on the xy-face 4-cycles of Q_3, whose four edges all lie in the disentangler bundle. The two xy-faces give the same Wilson exponent; the bottom face $z = 0$ is taken in canonical orientation $(000) \to (100) \to (110) \to (010) \to (000)$.

The face 4-cycle lives entirely in the xy-disentangler plane. All four edges of an xy-face are xy-bonds.

Incidence vector. Reading off signed edge contributions around the loop ($+1$ for positive traversal, -1 for reverse), with edge labels as in Appendix B,

$$b_L(e_2) = +1, \quad b_L(e_9) = +1, \quad b_L(e_6) = -1, \quad b_L(e_1) = -1, \tag{43}$$

and zero on the other eight edges. As a full vector in the edge basis $(e_0, \ldots, e_{11})$ of Appendix B,

$$b_L = (0, -1, +1, 0, 0, 0, -1, 0, 0, +1, 0, 0)^\top, \tag{44}$$

giving $|b_L|^2 = b_L^T b_L = 4$.

Bare Wilson flux. With the bare diagonal pinning $M_{ee} = \kappa_P = 32$ alone, the bare Wilson exponent is

$$\delta_L^{\text{bare}} := \tfrac{1}{2} b_L^T (\kappa_P I_{12})^{-1} b_L = \frac{|b_L|^2}{2\kappa_P} = \frac{4}{64} = \frac{1}{16}. \tag{45}$$

The Wilson loop is closed, so the recurrent formula (36) applies, giving the bare weak coupling

$$g_{L,\text{bare}}^2(m_P) = \frac{g^2(m_P)}{1 - 1/16} = \frac{g^2(m_P)}{15/16} = \tfrac{16}{15} g^2(m_P). \tag{46}$$

The off-diagonal disentangler structure of M refines this toward $g_L^2(m_P)$ in §4.

3.6 Hypercharge

The $U(1)_Y$ sector lives on the body diagonal of Q_3, the single line from (000) to (111) joining the two antipodal corners through the centre of the cube, sourced at its two endpoints where the external charges sit (Fig. 1). The diagonal is not an edge of Q_3; its edge representation is the staircase $(000) \to (100) \to (110) \to (111)$, the three edges e_2, e_9, e_{11}, one along each axis. The two in-plane steps are adjacent, the disentangler being a single operation on the xy-plane (§2.4), so the isometric z-step sits at an end and the staircase crosses one MERA layer; every staircase of this form gives the same Wilson exponent. The diagonal reaches the centre a distance $\sqrt{3}/2$ from each corner, the circumradius of the unit cube, and the edge representation carries this amplitude, $b_Y = \frac{\sqrt{3}}{2}(e_2 + e_9 + e_{11})$.

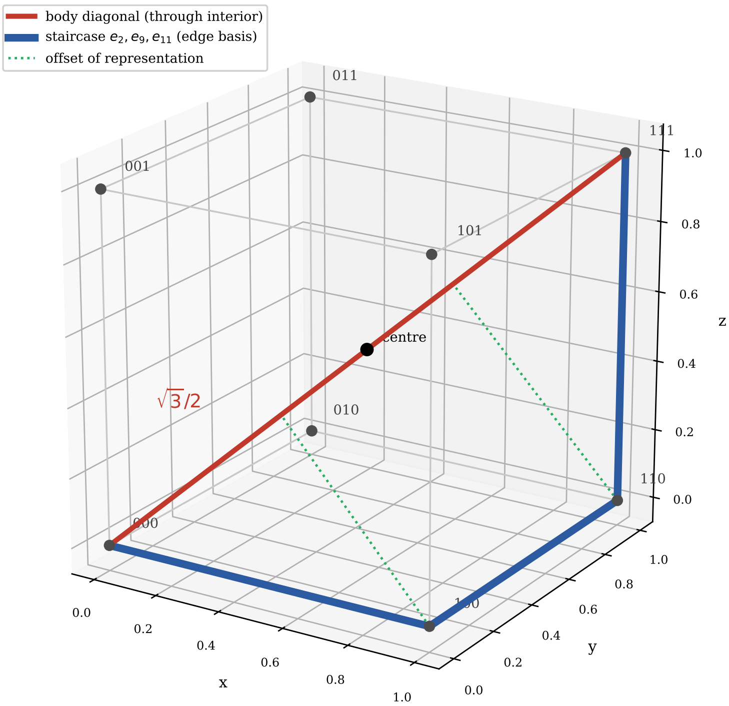

Figure 1: The hypercharge body diagonal (000)–(111) (red) through the centre of the cube, and its edge representation, the staircase e_2, e_9, e_{11} (blue). The diagonal reaches the centre a distance $\sqrt{3}/2$ from each corner, the circumradius of the unit cube; the edge representation carries this amplitude.

Incidence vector. The staircase edges carry the contour, each in positive orientation and weighted by the circumradius $\sqrt{3}/2$ of the through-centre diagonal:

$$b_Y = \frac{\sqrt{3}}{2}\big(e_2 + e_9 + e_{11}\big), \tag{47}$$

and zero on the other nine edges. As a full vector in the edge basis $(e_0, \dots, e_{11})$ of Appendix B,

$$b_Y = \frac{\sqrt{3}}{2}\,(0,0,1,0,0,0,0,0,0,1,0,1)^\top, \tag{48}$$

giving $|b_Y|^2 = b_Y^T b_Y = \frac{3}{4} \cdot 3 = \frac{9}{4}$.

Bare Wilson flux. With the bare diagonal pinning $M_{ee} = \kappa_P = 32$ alone, the bare Wilson exponent is

$$\delta_Y^{\text{bare}} := \tfrac{1}{2}\, b_Y^T (\kappa_P I_{12})^{-1} b_Y = \frac{|b_Y|^2}{2\kappa_P} = \frac{9/4}{64} = \frac{9}{256}. \tag{49}$$

The body diagonal is a Wilson line, so the transient formula (37) applies, giving the bare hypercharge coupling

$$g^2_{Y,\text{bare}}(m_P) \;=\; g^2(m_P)\left(1-\frac{9}{256}\right) \;=\; g^2(m_P)\cdot\frac{247}{256}. \tag{50}$$

The off-diagonal disentangler structure of M refines this toward $g^2_Y(m_P)$ in §4.

4 Disentangler deformations

The gauge couplings of §3 were computed without the disentangling step of the MERA, the local unitary that removes short-range entanglement before the isometric coarse-graining. The 1+2 split of §2.5 supplies the operators directly. The two disentangler axes x,y carry the in-plane disentangler, and the isometric axis z carries the isometric incidence; their composite enters the hypercharge correction. The gauge couplings close on the cube Q_3. With the disentangler off, the bond action is the diagonal pinning $M = \kappa_P I_{12}$, giving the bare quantities

$$g^2_{L,\text{bare}} = \tfrac{16}{15}\,g^2(m_P), \qquad g^2_{Y,\text{bare}} = \tfrac{247}{256}\,g^2(m_P). \tag{51}$$

4.1 The disentangler, the isometry, and their composite

The in-plane MERA disentanglers sit on the two diagonals of each xy face. Their projected effect on the bond action is the placement-weighted operator

$$D_{xy} = A_{xy} + 2\,P^{\square}_{xy}, \tag{52}$$

with A_{xy} the share-vertex in-plane part [17] and $P^{\square}_{xy}$ the opposite-parallel in-face part; the coefficient 2 records the two diagonal placements on each face. The isometric axis z carries the incidence operator I_z, joining each z-edge to the in-plane edges meeting it. The composite is the anticommutator

$$C = \{D_{xy}, I_z\} = D_{xy}I_z + I_z D_{xy}, \tag{53}$$

the symmetric bond-action representation of transport through both tensors of one MERA layer, the disentangler followed by the isometry. Each of D_{xy}, I_z, C is symmetric with vanishing diagonal, so the diagonal pinning $M_{ee} = \kappa_P = 32$ is preserved by every term. The explicit blocks are given in Appendix C.

Geometry of the three corrections. The three sectors are sorted by how their substrate sits relative to the xy-disentangler plane. The weak loop lies in that plane, on the four edges of an xy-face, so the disentangler acts on it directly through D_{xy}; this is the -8 moment (Appendix C). The hypercharge body diagonal runs from one corner of the cube through the centre to the opposite corner, crossing all three axes. In the edge basis it is the staircase $(000) \to (100) \to (110) \to (111)$ on e_2, e_9, e_{11}, with e_2, e_9 in the disentangler plane and e_{11} along the isometric axis. The in-plane segments couple to the disentangler, giving the moment $(b_Y)^{\mathsf{T}} D_{xy} b_Y = \frac{3}{2}$; the z segment couples to the isometric incidence, giving $(b_Y)^{\mathsf{T}} I_z b_Y = \frac{3}{2}$; and the transfer path linking the disentangler step to the isometry step across one MERA layer is the composite, the two orderings of $C = \{D_{xy}, I_z\}$, giving $(b_Y)^{\mathsf{T}} C\, b_Y = 6$. The strong sector runs along the z-edges, parallel to the isometry and perpendicular to the disentangler plane. The matching bundle carries no closed contour (§3.4), so $b_s = 0$ and $\delta_s = 0$ for any M.

4.2 The cube bond action and its deformation coefficients

On the cube the bond action carries the isometric incidence and the composite,

$$M_{Q_3} = \kappa_P \widetilde{M}, \qquad \widetilde{M} = I_{12} + c_I\, I_z - c_C\, C. \tag{54}$$

In the block basis (E_{xy}, E_z) the bracket matrix is

$$\widetilde{M} = \begin{pmatrix} I_8 & N \\ N^{\mathsf{T}} & I_4 \end{pmatrix}, \qquad N = c_I B - c_C DB, \tag{55}$$

with B the z-to-in-plane incidence block and DB the composite block, both listed in Appendix C.

The diagonal pinning $M_{ee} = \kappa_P$ makes every deformation traceless: no edge contributes to its own coefficient, and each coefficient is an open count over the edges its operator reaches. The cube isometric strength is the open star of the z-edge under I_z. Each z-edge meets four in-plane edges, two at each endpoint, so the row sum of I_z is 4 and $c_I = 4\xi^*$. The cube composite strength is the placement count of $D_{xy} = A_{xy} + 2P_{xy}^{\square}$. The flip $x \mapsto 1-x$ is an automorphism of Q_3 exchanging the two diagonals of every xy-face, so the two placements carry equal weight, and a placement enters an incidence operator by its multiplicity. The composite block DB has row sum $8 = 2\times 4$, twice the incidence, so $c_C = 2\xi^*$, the two diagonal placements on each face inherited from D_{xy},

$$c_I = 4\xi^*, \qquad c_C = 2\xi^*. \tag{56}$$

Each coefficient is a geometric count carried at the residual entanglement capacity ξ^* per bond, $\xi^* = \log\chi - S^* = 1/36$ of (10). The spectrum of $\widetilde{M}$ is

$$\operatorname{spec}(\widetilde{M}) = \{0.556^{(2)}, 0.686, 1^{(6)}, 1.314, 1.444^{(2)}\}, \tag{57}$$

so $\lambda_{\min}(\widetilde{M}) = 0.556 > 0$ and $\lambda_{\min}(M_{Q_3}) = 32 \times 0.556 = 17.78 > 0$; the bond action is positive-definite. Written out in the block basis $(e_1, e_2, e_3, e_4, e_6, e_7, e_9, e_{10}, e_0, e_5, e_8, e_{11})$, with diagonal $\kappa_P = 32$ and off-diagonal entries $32c_I - 32c_C = 32(0.055556) = 1.7778$ and $-32c_C \cdot 3 = 32(-0.166667) = -5.3333$, the full matrix is

$$M_{Q_3} = \begin{pmatrix}
32 & 0 & 0 & 0 & 0 & 0 & 0 & 0 & 1.7778 & 1.7778 & -5.3333 & -5.3333 \\
0 & 32 & 0 & 0 & 0 & 0 & 0 & 0 & 1.7778 & -5.3333 & 1.7778 & -5.3333 \\
0 & 0 & 32 & 0 & 0 & 0 & 0 & 0 & 1.7778 & 1.7778 & -5.3333 & -5.3333 \\
0 & 0 & 0 & 32 & 0 & 0 & 0 & 0 & 1.7778 & -5.3333 & 1.7778 & -5.3333 \\
0 & 0 & 0 & 0 & 32 & 0 & 0 & 0 & -5.3333 & 1.7778 & -5.3333 & 1.7778 \\
0 & 0 & 0 & 0 & 0 & 32 & 0 & 0 & -5.3333 & 1.7778 & -5.3333 & 1.7778 \\
0 & 0 & 0 & 0 & 0 & 0 & 32 & 0 & -5.3333 & -5.3333 & 1.7778 & 1.7778 \\
0 & 0 & 0 & 0 & 0 & 0 & 0 & 32 & -5.3333 & -5.3333 & 1.7778 & 1.7778 \\
1.7778 & 1.7778 & 1.7778 & 1.7778 & -5.3333 & -5.3333 & -5.3333 & -5.3333 & 32 & 0 & 0 & 0 \\
1.7778 & -5.3333 & 1.7778 & -5.3333 & 1.7778 & 1.7778 & -5.3333 & -5.3333 & 0 & 32 & 0 & 0 \\
-5.3333 & 1.7778 & -5.3333 & 1.7778 & -5.3333 & -5.3333 & 1.7778 & 1.7778 & 0 & 0 & 32 & 0 \\
-5.3333 & -5.3333 & -5.3333 & -5.3333 & 1.7778 & 1.7778 & 1.7778 & 1.7778 & 0 & 0 & 0 & 32
\end{pmatrix}. \tag{58}$$

The couplings of the three gauge sectors are read from it through the matching-vector quadratic forms $\delta_G = \frac{1}{2} b_G^{\mathsf{T}} M_{Q_3}^{-1} b_G$, with $g^2 = g^2(m_P)$ the unmodified coupling; the inverse is listed in Appendix D.

4.3 The strong coupling

The strong matching vector vanishes in the deformation sector, $b_s = 0$, so

$$\delta_s = \tfrac{1}{2} b_s^{\mathsf{T}} M_{Q_3}^{-1} b_s = 0, \qquad g_s^2(m_P) = g^2(m_P). \tag{59}$$

4.4 The weak coupling

The weak matching vector b_L gives the exponent and recurrent coupling

$$\delta_L = \tfrac{1}{2} b_L^{\mathsf{T}} M_{Q_3}^{-1} b_L = 0.070192, \qquad g_L^2(m_P) = \frac{g^2}{1-\delta_L}. \tag{60}$$

Because b_L is supported on the four edges e_1, e_2, e_6, e_9 with entries $(-1, +1, -1, +1)$, the quadratic form uses only the 4×4 principal submatrix of $M_{Q_3}^{-1}$ on those edges,

$$\left(M_{Q_3}^{-1}\right)_{\{e_1,e_2,e_6,e_9\}} = \begin{pmatrix}
0.033601 & 0.000428 & 0.000428 & -0.001495 \\
0.000428 & 0.033601 & -0.001495 & 0.000428 \\
0.000428 & -0.001495 & 0.033601 & 0.000428 \\
-0.001495 & 0.000428 & 0.000428 & 0.033601
\end{pmatrix}. \tag{61}$$

Contracting with the entries $(-1,+1,-1,+1)$ of b_L on this support, the four diagonal terms give $4(0.033601) = 0.134405$ and the off-diagonal terms add 0.005980, so $b_L^{\mathsf{T}} M_{Q_3}^{-1} b_L = 0.140385$ and $\delta_L = \frac{1}{2}(0.140385) = 0.070192$.

4.5 The hypercharge coupling

The hypercharge contour is the body diagonal of §3.6, the same staircase $b_Y = \frac{\sqrt{3}}{2}(e_2 + e_9 + e_{11})$ used bare and deformed, with no change of contour between the two. The hypercharge line b_Y gives the exponent and transient coupling

$$\delta_Y = \tfrac{1}{2}\,(b_Y)^{\mathsf{T}} M_{Q_3}^{-1} b_Y = 0.041894, \qquad g_Y^2(m_P) = g^2(1-\delta_Y). \tag{62}$$

The line b_Y is supported on e_2, e_9, e_{11} with the circumradius weight $\sqrt{3}/2$, so the quadratic form uses the 3×3 principal submatrix of $M_{Q_3}^{-1}$ on those three edges,

$$\left(M_{Q_3}^{-1}\right)_{\{e_2,e_9,e_{11}\}} = \begin{pmatrix} 0.033601 & 0.000428 & 0.006253 \\ 0.000428 & 0.033601 & -0.002401 \\ 0.006253 & -0.002401 & 0.035952 \end{pmatrix}, \tag{63}$$

giving $(b_Y)^{\mathsf{T}} M_{Q_3}^{-1} b_Y = \frac{3}{4}\left[0.033601 + 0.033601 + 0.035952 + 2(0.000428 + 0.006253 - 0.002401)\right] = \frac{3}{4}(0.111716) = 0.083787$ and $\delta_Y = \frac{1}{2}(0.083787) = 0.041894$. The weak loop and the hypercharge line contract the three operators to the six moments

$$\begin{aligned} b_L^{\mathsf{T}} D_{xy} b_L &= -8, & (b_Y)^{\mathsf{T}} D_{xy} b_Y &= \tfrac{3}{2}, \\ b_L^{\mathsf{T}} I_z b_L &= 0, & (b_Y)^{\mathsf{T}} I_z b_Y &= \tfrac{3}{2}, \\ b_L^{\mathsf{T}} C\, b_L &= 0, & (b_Y)^{\mathsf{T}} C\, b_Y &= 6, \end{aligned} \tag{64}$$

derived in full in Appendix C. The staircase representation of the body diagonal crosses all three axes, so the hypercharge line couples to the in-plane disentangler and the isometric incidence through its xy and z segments, and to the composite through the transfer path linking the two across one MERA layer.

5 The entanglement oscillator bond action against the PDG data

quantity	PDG/Buttazzo reference	bare	bond action
$g_s^2(m_P)$	0.237350	0.237350 (input)	0.237350 (input)
$g_L^2(m_P)$	0.255530	0.253173 (-0.92%)	0.255268 (-0.10%)
$g_Y^2(m_P)$	0.227535	0.229006 $(+0.65\%)$	0.227406 (-0.056%)
$\sin^2\theta_W(m_P)$	0.47102	0.474939 $(+0.83\%)$	0.47114 $(+0.025\%)$
	$M_{Q_3} = \kappa_P\left[I_{12} + \xi^*(4I_z - 2C)\right]$ (bond action)		

Table 5: The three gauge couplings and the weak mixing angle at the Planck scale. The reference column is the PDG 2024 [13] inputs $M_t = 172.57$ GeV, $M_W = 80.369$ GeV, $\alpha_s(M_Z) = 0.1180$ run to m_P via Buttazzo eq.(61) [14]; $g_Y^2 = \frac{3}{5}g_1^2$ is the physical hypercharge, from the GUT-normalized g_1 of eq.(61). $g_s^2(m_P)$ is the single input and closes by construction; the deformation predicts g_L^2, g_Y^2, and $\sin^2\theta_W$, with residuals against the reference column. The bare column is the diagonal pinning alone, $g_{L,\text{bare}}^2 = \frac{16}{15}g^2$ and $g_{Y,\text{bare}}^2 = \frac{247}{256}g^2$ at $g^2 = g_s^2(m_P)$; the bond action column completes the deformation.

6 From gauge to energy scales, the prism

The cube Q_3 carried the gauge sectors and, under the disentangler deformation, the gravitational constant. The prism Q_4, developed in the Emergent Gravity section below as the temporal geometry whose propagator trace closes G_N, now becomes the full setting for the energy scales of the theory. Extending Q_3 along the temporal axis τ produces Q_4 (Fig. 2); the electroweak vacuum expectation value, the Higgs field, and the confining string tension are all read from operators on this prism.

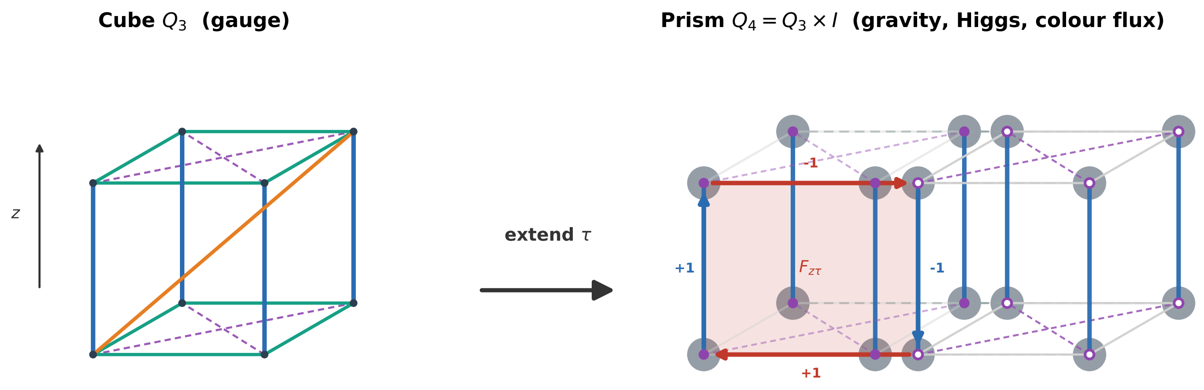

Figure 2: From the cube to the prism. On the cube Q_3 the gauge sectors sit on the geometry, the $\mathrm{SU}(3)_c$ colour axis on the z-edges, $\mathrm{SU}(2)_L$ on the xy-face loops, $\mathrm{U}(1)_Y$ on the body diagonal. The temporal axis τ carries the cube to the prism $Q_4 = Q_3 \times I$, two cube copies at $\tau = 0$ and $\tau = 1$. On the prism the gravitational constant is the whole vertex trace, the Higgs field is the temporal vertex mode, and the string tension is the colour flux on the $z\tau$-face.

Two facts are used here, one from the gauge sections above, one from the Emergent Gravity section below. First, the Bekenstein–Hawking bound $\log\chi = 1/4$ gives the vacuum entanglement $S^* = N\log\chi/(N+1) = 2/9$ and the residual capacity $\xi^* = \log\chi - S^* = 1/36$; these three quantities, derived in the vacuum entanglement and eigenvalue-scan sections above, set every scale below. Second, the deformed prism trace derived in the Emergent Gravity section below gives $\Sigma_V = 3.82333$ and $G_N = 0.999057\,\ell_P^2$. The vacuum expectation value is a spectral projection against this trace, the string tension against the edge trace of the same prism. The energy scales are thus not a separate construction. They are projections of the one geometry that produced the gauge couplings and the gravitational constant.

7 The prism and its operators

The prism is the four-cube graph $Q_4 = Q_3 \times I$, the Cartesian product of four single edges, one per cube axis x, y, z and one for the temporal direction τ. Its vertices are the four-bit strings (x, y, z, τ), sixteen in number, two joined when their strings differ in one bit.

7.1 The vertex operator

The scalar operator is the vertex Laplacian with a unit mass shift,

$$M_0 = L_0 + I, \qquad L_0 = D_0 - A, \tag{65}$$

with A the vertex adjacency matrix and $D_0 = 4I$ the degree. The deformed operator is its weighted counterpart,

$$M_\omega = L_\omega + I, \tag{66}$$

so $\mathrm{spec}(M_\omega) = \mathrm{spec}(L_\omega) + 1$ and the trace of its inverse is the sum over the shifted eigenvalues, $\mathrm{Tr}\, M_\omega^{-1} = \sum_n 1/(\lambda_n + 1)$. The single edge K_2 has Laplacian

$$L_{K_2} = \begin{pmatrix} 1 & -1 \\ -1 & 1 \end{pmatrix}, \qquad \mathrm{spec}(L_{K_2}) = \{0, 2\}. \tag{67}$$

For a Cartesian product the Laplacian is the Kronecker sum of the factor Laplacians [17], so the eigenvalues of $Q_4 = K_2^{\square 4}$ are the four-fold sums of the K_2 eigenvalues. As a Cartesian product of four single edges, each contributing eigenvalue 0 or 2, the spectrum of L_0 is set by the number $k \in \{0, \dots, 4\}$ of factors contributing 2, equal to $2k$, with multiplicity $\binom{4}{k}$,

$$\mathrm{spec}(L_0) = \{0^{(1)}, 2^{(4)}, 4^{(6)}, 6^{(4)}, 8^{(1)}\}, \tag{68}$$

the multiplicities $(1,4,6,4,1) = \binom{4}{k}$, in agreement with direct diagonalisation of L_0. The matrices A, L_0, and M_0 are written out in Appendix E.

7.2 The edge operator

The edge operator is the edge Laplacian, built from the same coboundary that builds the vertex Laplacian. Orient each edge from its 0-vertex to its 1-vertex in the flipped bit, and let d_0 be the coboundary, the discrete gradient, from the sixteen vertices to the thirty-two edges, $(d_0 f)_e = f(\text{head}) - f(\text{tail})$, a 32×16 matrix; its transpose $d_0^\top$ is the boundary. The vertex Laplacian is the composition $d_0^\top d_0$: for a vertex function f, $(d_0^\top d_0 f)_v = \sum_{e \ni v} \pm (f(\text{head}) - f(\text{tail})) = \deg(v) f(v) - \sum_{u \sim v} f(u) = (L_0 f)_v$, so

$$L_0 = d_0^\top d_0. \tag{69}$$

The edge Laplacian is the other composition, acting on vectors on the edges,

$$M_1 = L_1 + I, \qquad L_1 = d_0 d_0^\top, \tag{70}$$

a 32×32 operator. The two compositions $d_0^\top d_0$ and $d_0 d_0^\top$ share the same nonzero eigenvalues, the squared singular values of d_0: if $d_0^\top d_0 \phi = \lambda \phi$ with $\lambda \neq 0$ then $d_0 d_0^\top (d_0 \phi) = \lambda (d_0 \phi)$, the map $\phi \mapsto d_0 \phi$ carrying the nonzero eigenvectors of L_0 to those of L_1. So the nonzero spectrum of L_1 is that of L_0, namely $\{2^{(4)}, 4^{(6)}, 6^{(4)}, 8^{(1)}\}$. The rank of d_0 is the number of vertices less the connected components, $16 - 1 = 15$, so the kernel of L_1, the cycle space $\ker d_0^\top$ (harmonic for the down-Laplacian $d_0 d_0^\top$, there being no 2-cells), has dimension $32 - 15 = 17$, and

$$\mathrm{spec}(L_1) = \{0^{(17)}, 2^{(4)}, 4^{(6)}, 6^{(4)}, 8^{(1)}\}. \tag{71}$$

The coboundary d_0 and the edge operator L_1 are written out in Appendix E.

8 Emergent Gravity

Gravity here is induced, not fundamental. The mechanism is Sakharov's. A matter field on a fixed background is integrated out, and its vacuum fluctuations generate an Einstein–Hilbert term for the metric [11, 20]. Related programs treat gravity as thermodynamic or entropic in origin [21, 22]. The matter is the bond-oscillator scalar on the prism $Q_3 \times I$, integrated out at the Planck-scale mass $m = m_P$.

8.1 The Sakharov mechanism

The modern heat-kernel form of the scalar Sakharov coefficient is[1]

$$\frac{1}{16\pi G_N} = \frac{1}{12} \int_0^\infty ds \int \frac{d^4k}{(2\pi)^4} e^{-s(k^2+m^2)}. \tag{72}$$

[1] The factor $1/12$ is the standard scalar coefficient. $1/2$ comes from the real-scalar one-loop determinant and $1/6$ from the scalar curvature term in the heat-kernel coefficient; see Refs. [20, 23, 24, 25].

The proper-time integral gives the Euclidean momentum-space scalar propagator,

$$\int_0^\infty ds\, e^{-s(k^2+m^2)} = \frac{1}{k^2+m^2}, \tag{73}$$

so the induced coefficient becomes

$$\frac{1}{16\pi G_N} = \frac{1}{12}\int \frac{d^4k}{(2\pi)^4}\frac{1}{k^2+m^2}. \tag{74}$$

The volume factor enters when this continuum propagator integral is represented by a finite spectral sum. The continuum integral is the mode density per unit four-volume, so its discrete counterpart is the finite sum over modes divided by the four-volume the modes occupy,

$$\int \frac{d^4k}{(2\pi)^4}\frac{1}{k^2+m^2} \longrightarrow \frac{1}{V}\sum_n \frac{1}{\lambda_n+m^2}, \tag{75}$$

with V the physical four-volume set below by the mode density. Thus the finite spectral form of the scalar Sakharov coefficient is

$$\frac{1}{16\pi G_N} = \frac{1}{12}\,\frac{1}{V}\sum_n \frac{1}{\lambda_n+m^2}. \tag{76}$$

The scalar matter operator on Q_4 is

$$M_{Q_4} = \Delta_{Q_4} + m^2 I = \ell_P^{-2}\widetilde{\Delta}_{Q_4} + m^2 I, \qquad m = m_P = \ell_P^{-1}. \tag{77}$$

Here $\widetilde{\Delta}_{Q_4} = L_0$ is the dimensionless scalar graph Laplacian on the 16 prism vertices, and $\Delta_{Q_4} = \ell_P^{-2}\widetilde{\Delta}_{Q_4}$ is the corresponding physical Laplacian.

The prism $Q_3\times I$ is the 4-cube graph $Q_4 = K_2^{\square 4}$, the Cartesian product of four single edges, one per cube axis and one for the temporal direction. Labelling each vertex by the 4-bit string (x,y,z,τ), so that $v = 8x+4y+2z+\tau$, two vertices are joined when their strings differ in one bit, so every vertex has degree 4 and $D = 4I_{16}$. Ordering the vertices $0000, 0001, \ldots, 1111$, the adjacency matrix is

$$A = \begin{pmatrix}
0&1&1&0&1&0&0&0&1&0&0&0&0&0&0&0\\
1&0&0&1&0&1&0&0&0&1&0&0&0&0&0&0\\
1&0&0&1&0&0&1&0&0&0&1&0&0&0&0&0\\
0&1&1&0&0&0&0&1&0&0&0&1&0&0&0&0\\
1&0&0&0&0&1&1&0&0&0&0&0&1&0&0&0\\
0&1&0&0&1&0&0&1&0&0&0&0&0&1&0&0\\
0&0&1&0&1&0&0&1&0&0&0&0&0&0&1&0\\
0&0&0&1&0&1&1&0&0&0&0&0&0&0&0&1\\
1&0&0&0&0&0&0&0&0&1&1&0&1&0&0&0\\
0&1&0&0&0&0&0&0&1&0&0&1&0&1&0&0\\
0&0&1&0&0&0&0&0&1&0&0&1&0&0&1&0\\
0&0&0&1&0&0&0&0&0&1&1&0&0&0&0&1\\
0&0&0&0&1&0&0&0&1&0&0&0&0&1&1&0\\
0&0&0&0&0&1&0&0&0&1&0&0&1&0&0&1\\
0&0&0&0&0&0&1&0&0&0&1&0&1&0&0&1\\
0&0&0&0&0&0&0&1&0&0&0&1&0&1&1&0
\end{pmatrix}, \tag{78}$$

and the Laplacian $L_0 = 4I_{16} - A$ is

$$L_0 = \begin{pmatrix}
4&-1&-1&0&-1&0&0&0&-1&0&0&0&0&0&0&0\\
-1&4&0&-1&0&-1&0&0&0&-1&0&0&0&0&0&0\\
-1&0&4&-1&0&0&-1&0&0&0&-1&0&0&0&0&0\\
0&-1&-1&4&0&0&0&-1&0&0&0&-1&0&0&0&0\\
-1&0&0&0&4&-1&-1&0&0&0&0&0&-1&0&0&0\\
0&-1&0&0&-1&4&0&-1&0&0&0&0&0&-1&0&0\\
0&0&-1&0&-1&0&4&-1&0&0&0&0&0&0&-1&0\\
0&0&0&-1&0&-1&-1&4&0&0&0&0&0&0&0&-1\\
-1&0&0&0&0&0&0&0&4&-1&-1&0&-1&0&0&0\\
0&-1&0&0&0&0&0&0&-1&4&0&-1&0&-1&0&0\\
0&0&-1&0&0&0&0&0&-1&0&4&-1&0&0&-1&0\\
0&0&0&-1&0&0&0&0&0&-1&-1&4&0&0&0&-1\\
0&0&0&0&-1&0&0&0&-1&0&0&0&4&-1&-1&0\\
0&0&0&0&0&-1&0&0&0&-1&0&0&-1&4&0&-1\\
0&0&0&0&0&0&-1&0&0&0&-1&0&-1&0&4&-1\\
0&0&0&0&0&0&0&-1&0&0&0&-1&0&-1&-1&4
\end{pmatrix}. \tag{79}$$

The spectrum follows from the product structure. The single edge K_2 has Laplacian

$$L_{K_2} = \begin{pmatrix} 1 & -1 \\ -1 & 1 \end{pmatrix}, \qquad \mathrm{spec}(L_{K_2}) = \{0, 2\}. \tag{80}$$

For a Cartesian product the Laplacian is the Kronecker sum of the factor Laplacians, so the eigenvalues of $Q_4 = K_2^{\square 4}$ are the four-fold sums of the K_2 eigenvalues. An eigenvalue is set by the number $k \in \{0, \ldots, 4\}$ of factors contributing 2, equal to $2k$, and the number of ways to choose those factors is $\binom{4}{k}$. The spectrum of L_0 is finite,

$$\mathrm{spec}(L_0) \;=\; \{0,\, 2^{(4)},\, 4^{(6)},\, 6^{(4)},\, 8^{(1)}\}, \tag{81}$$

the multiplicities $(1,4,6,4,1) = \binom{4}{k}$, in agreement with direct diagonalisation of L_0 in (79). There are 16 modes, with maximum eigenvalue $\lambda_{\max} = 8$. There is no scale shorter than one bond, so the spectrum terminates. The heat trace is therefore finite as $s \to 0$,

$$\mathrm{Tr}\, e^{-sM} \;=\; \sum_n e^{-s(\lambda_n + m^2)} \xrightarrow{s\to 0} N \;=\; 16, \tag{82}$$

The spectrum in (81) contains

$$N = 1+4+6+4+1 = 16 \tag{83}$$

finite scalar modes. This is the trace dimension, not by itself the physical four-volume. The heat-kernel density requires a physical normalization volume. For the Planck prism this normalization is one finite scalar mode per Planck four-volume,

$$\frac{N}{V_{\text{prism}}} = \ell_P^{-4}. \tag{84}$$

Since $N = 16$,

$$V_{\text{prism}} = 16\,\ell_P^4. \tag{85}$$

The graph-Laplacian eigenvalues $\tilde{\lambda}_n$ are dimensionless, while in physical units

$$\lambda_n = \frac{\tilde{\lambda}_n}{\ell_P^2}, \qquad m = m_P = \ell_P^{-1}, \qquad \frac{1}{\lambda_n + m^2} = \frac{\ell_P^2}{\tilde{\lambda}_n + 1}. \tag{86}$$

Substituting (85) and (86) into (76) gives

$$\frac{1}{16\pi G_N} = \frac{1}{12}\,\frac{1}{16\ell_P^4}\sum_n \frac{\ell_P^2}{\tilde{\lambda}_n + 1}. \tag{87}$$

Using the multiplicities in (81),

$$\sum_n \frac{1}{\tilde{\lambda}_n + 1} = 1 + \frac{4}{3} + \frac{6}{5} + \frac{4}{7} + \frac{1}{9} = 4.215873. \tag{88}$$

Therefore

$$\frac{1}{16\pi G_N} = \frac{4.215873}{192}\,\ell_P^{-2} = 0.021958\,\ell_P^{-2}. \tag{89}$$

Solving for G_N,

$$G_N = \frac{1}{16\pi(0.021958)}\,\ell_P^2 = 0.906033\,\ell_P^2, \tag{90}$$

in Einstein–Hilbert normalisation.

Position in the literature. Continuum implementations of Sakharov's mechanism [20, 26, 27, 28] yield G_N only to the magnitude of an imposed cutoff. Graph-theoretic and dimensional-deconstruction models obtain a finite induced G_N only after choosing the matter content so that bosonic and fermionic divergences cancel. A single scalar on a finite spectrum, with no cancellation and no cutoff, gives an induced gravitational constant of order ℓ_P^2. In the present setting the prism spectrum, the trace-density normalization, and the Planck-scale mass are all specified by the construction rather than by a cutoff.

The value $G_N = 0.906\,\ell_P^2$ is the bare result.

8.2 The disentangler deformation

The gravitational physics develops on the prism Q_4, $|V(Q_4)| = 16$, the cube extended by the temporal direction τ. It is a different graph from the gauge cube, and the deformation enters it through the prism edge weights set by the in-plane disentangler,

$$\omega_k = 1 + c_D \left(D_{xy}^{(Q_4)}\mathbf{1}\right)_k. \tag{91}$$

$\left(D_{xy}^{(Q_4)}\mathbf{1}\right)_k$ being the row sum of the prism disentangler at edge k. The prism coefficient c_D is not independent. The prism $Q_4 = Q_3 \times I$ is two copies of the cube, at $\tau = 0$ and $\tau = 1$, so the in-plane disentangler on the prism is the cube disentangler acting in each copy, tensored with the two-element interval,

$$D_{xy}^{(Q_4)} = D_{xy}^{(Q_3)} \otimes I_2. \tag{92}$$

The eigenvalues of the cube disentangler $D_{xy}^{(Q_3)}$ on the (x,y) bundle (Appendix C) are $\{-2^{(4)}, 0^{(2)}, 4^{(2)}\}$, and the tensor with I_2 doubles each multiplicity to $\{-2^{(8)}, 0^{(4)}, 4^{(4)}\}$ on the prism. The prism composite strength comes from §2.5. The per-bond residual capacity, the room the vacuum leaves below the Bekenstein–Hawking bound, is $\xi^* = \log\chi - S^* = \frac{1}{4} - \frac{2}{9} = \frac{1}{36}$. The deformation enters through the edge weights ω_k themselves, so its cell is closed: each edge belongs to its own count. The cell is the support of one MERA layer, the isometric edge carrying the isometry together with the four in-plane edges meeting its endpoints, where the disentangler faces attach—the closed star of an isometric edge, five edges (Fig. 3). The τ-edges carry neither tensor, $D_{xy}^{(Q_4)} = D_{xy}^{(Q_3)} \otimes I_2$ acting per copy and the isometry along z, so the cell is the same five edges in each copy. With ξ^* per bond, the cell carries $5\,\xi^*$. The weights are conductances, one per edge, summed at the vertices, and the conductance of a bond of fixed makeup is inverse to its length, the unit edges calibrating weight one at length one. The disentanglers deliver the cell strength through the face diagonals, of length $\sqrt{2}$ in units of the edge, so the count carried by the star enters the weight per unit diagonal,

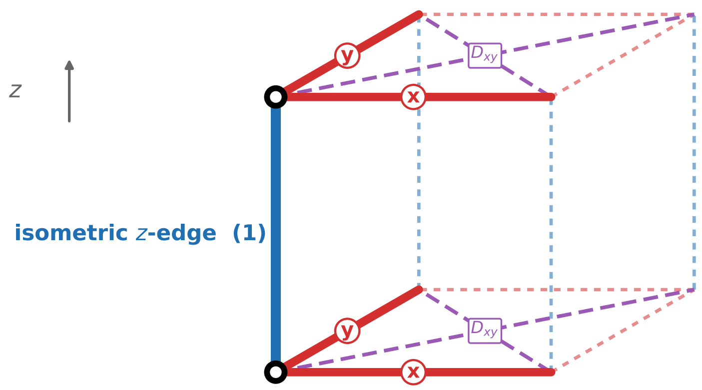

Figure 3: The closed star of an isometric edge, five edges. Solid lines are the five edges of the star, the isometric z-edge (blue, labelled 1) together with the four in-plane edges (red) meeting its two endpoints, two at each degree-three vertex. The disentanglers D_{xy} act on both face diagonals of each x,y-face (purple, dashed). The remaining cube edges are shown by type, z (blue) and x,y (red).

$$c_D = \frac{5}{\sqrt{2}}\,\xi^* = 0.098209. \tag{93}$$

With c_D in hand, on the prism the row sum is 4 on each in-plane edge and 0 on the z and temporal edges, so

$$\omega_k = 1 + 4\,c_D = 1.3928 \ \text{(in-plane edges)}, \qquad \omega_k = 1 \ \ (z \text{ and temporal edges}). \tag{94}$$

The weighted vertex Laplacian $(L_\omega)_{ii} = \sum_{k\ni i}\omega_k$, $(L_\omega)_{ij} = -\sum_{k=(i,j)}\omega_k$, with vertices ordered $0000, 0001, \ldots, 1111$, diagonal $2(1.3928) + 2(1) = 4.7857$ at every vertex (each meets two in-plane edges of weight 1.3928 and two z/temporal edges of weight 1) and off-diagonal -1.3928 on in-plane edges, -1 on z/temporal edges, is

$$L_\omega = \begin{pmatrix}
4.786 & -1 & -1 & 0 & -1.393 & 0 & 0 & 0 & -1.393 & 0 & 0 & 0 & 0 & 0 & 0 & 0\\
-1 & 4.786 & 0 & -1 & 0 & -1.393 & 0 & 0 & 0 & -1.393 & 0 & 0 & 0 & 0 & 0 & 0\\
-1 & 0 & 4.786 & -1 & 0 & 0 & -1.393 & 0 & 0 & 0 & -1.393 & 0 & 0 & 0 & 0 & 0\\
0 & -1 & -1 & 4.786 & 0 & 0 & 0 & -1.393 & 0 & 0 & 0 & -1.393 & 0 & 0 & 0 & 0\\
-1.393 & 0 & 0 & 0 & 4.786 & -1 & -1 & 0 & 0 & 0 & 0 & 0 & -1.393 & 0 & 0 & 0\\
0 & -1.393 & 0 & 0 & -1 & 4.786 & 0 & -1 & 0 & 0 & 0 & 0 & 0 & -1.393 & 0 & 0\\
0 & 0 & -1.393 & 0 & -1 & 0 & 4.786 & -1 & 0 & 0 & 0 & 0 & 0 & 0 & -1.393 & 0\\
0 & 0 & 0 & -1.393 & 0 & -1 & -1 & 4.786 & 0 & 0 & 0 & 0 & 0 & 0 & 0 & -1.393\\
-1.393 & 0 & 0 & 0 & 0 & 0 & 0 & 0 & 4.786 & -1 & -1 & 0 & -1.393 & 0 & 0 & 0\\
0 & -1.393 & 0 & 0 & 0 & 0 & 0 & 0 & -1 & 4.786 & 0 & -1 & 0 & -1.393 & 0 & 0\\
0 & 0 & -1.393 & 0 & 0 & 0 & 0 & 0 & -1 & 0 & 4.786 & -1 & 0 & 0 & -1.393 & 0\\
0 & 0 & 0 & -1.393 & 0 & 0 & 0 & 0 & 0 & -1 & -1 & 4.786 & 0 & 0 & 0 & -1.393\\
0 & 0 & 0 & 0 & -1.393 & 0 & 0 & 0 & -1.393 & 0 & 0 & 0 & 4.786 & -1 & -1 & 0\\
0 & 0 & 0 & 0 & 0 & -1.393 & 0 & 0 & 0 & -1.393 & 0 & 0 & -1 & 4.786 & 0 & -1\\
0 & 0 & 0 & 0 & 0 & 0 & -1.393 & 0 & 0 & 0 & -1.393 & 0 & -1 & 0 & 4.786 & -1\\
0 & 0 & 0 & 0 & 0 & 0 & 0 & -1.393 & 0 & 0 & 0 & -1.393 & 0 & -1 & -1 & 4.786
\end{pmatrix} \tag{95}$$

with the sixteen eigenvalues

$$\operatorname{spec}(L_\omega) = \{0,\, 2^{(2)},\, 2.7857^{(2)},\, 4,\, 4.7857^{(4)},\, 5.5713,\, 6.7857^{(2)},\, 7.5713^{(2)},\, 9.5713\}. \tag{96}$$

The scalar operator of (77) is $\Delta_{Q_4} + m^2 I$.

The gravitational constant is the prism proper-time integral

$$\frac{1}{16\pi G_N} = \frac{1}{12}\,\frac{1}{16\,\ell_P^2}\sum_n \frac{1}{\lambda_n + 1}. \tag{97}$$

The spectral sum, term by term over the distinct eigenvalues, is

$$\sum_n \tfrac{1}{\lambda_n+1} = \tfrac{1}{1} + \tfrac{2}{3} + \tfrac{2}{3.7857} + \tfrac{1}{5} + \tfrac{4}{5.7857} + \tfrac{1}{6.5713} + \tfrac{2}{7.7857} + \tfrac{2}{8.5713} + \tfrac{1}{10.5713} = 3.82333, \tag{98}$$

giving

$$\frac{1}{16\pi G_N} = \frac{3.82333}{192}\,\ell_P^{-2} = 0.019913\,\ell_P^{-2}, \qquad G_N = 0.999057\,\ell_P^2. \tag{99}$$

The prism factorises as the (x,y)-square, the z-edge, and the temporal edge, so each eigenvalue of L_ω is the sum of the three factor eigenvalues, the in-plane factor scaled by the in-plane weight,

$$\lambda = \omega_k\,\mu_{xy} + \mu_z + \mu_\tau, \qquad \mu_{xy} \in \{0,2,4\} \text{ mult } \{1,2,1\}, \quad \mu_z, \mu_\tau \in \{0,2\}. \tag{100}$$

The gravitational constant then follows from the weight alone,

$$\frac{1}{16\pi G_N} = \frac{1}{12}\,\frac{1}{16\,\ell_P^2}\sum_{\mu_{xy},\mu_z,\mu_\tau} \frac{m(\mu_{xy})}{\omega_k\,\mu_{xy} + \mu_z + \mu_\tau + 1}. \tag{101}$$

At $\omega_k = 1$ this returns the bare $G_N^{\mathrm{bare}} = 0.906033\,\ell_P^2$. At $\omega_k = 1.3928$ it gives $G_N = 0.999057\,\ell_P^2$.

9 The master equation

The gravitational constant is the whole trace of the vertex operator. The vacuum expectation value is a single mode of that operator, the Higgs field. The string tension is the colour flux on the edge operator. It is proposed that these two are carried from the Planck scale to the infrared by the descent,

$$\text{scale} \;=\; m_P\, \Theta\, \Pi^p\, \exp\!\Big(-\frac{1}{\xi^*}\Big) \tag{102}$$

The exponential $\exp(-1/\xi^*)$ is the descent suppression, the saddle of the temporal-mode action. The colour representation factor Θ is the trace of the identity over the colour charge the object carries, over the channels it propagates through. The spectral weight Π is the mode's propagator weight against the whole trace, raised to the number p of field factors, one for a scalar and two for a vector. The three factors are developed in the next three sections and applied to the two scales after.

9.1 Descent

The exponent is the saddle value of the temporal-mode action along the descent. The descent is scale-invariant, one layer map repeated, so the temporal amplitude a_k at layer k is carried by the surviving site fraction,

$$a_k = f\, a_{k-1}, \qquad f = \frac{N}{N+1} = \frac{S^*}{\log\chi} = \frac{8}{9}, \tag{103}$$

the fraction being the vacuum entanglement over the bound, $f = N/(N+1) = [N\log\chi/(N+1)]/\log\chi = S^*/\log\chi$, with saddle profile $a_k = f^k$ from the unit initial value $a_0 = 1$. The temporal contour is open, its boundary nonzero at every vertex, so it couples to the bond field as a linear source through the entropic metric $1/\log\chi$ of the bound (1), and the descent action is the recurrence constraint and the open source,

$$S[\{a_k\}] = \frac{1}{2\log\chi}\sum_k \big(a_k - f\, a_{k-1}\big)^2 + \frac{1}{\log\chi}\sum_k a_k. \tag{104}$$

Both terms carry the entropic metric $1/\log\chi$, so the source enters at the same strength as the recurrence constraint. The Euler–Lagrange equation of the first term, $(a_k - fa_{k-1}) - f(a_{k+1} - fa_k) = 0$, is solved termwise by the recurrence (103), on which the first term vanishes. The open source has no quadratic counterterm because the contour is open; a closed contour would give a quadratic source $\sum_k f^{2k}$ and a different value. On the saddle profile $a_k = f^k$ the first term is zero and the action is the source summed over the descent,

$$S_{\text{eff}} = \frac{1}{\log\chi}\sum_{k=0}^{\infty} f^k = \frac{1}{\log\chi}\,\frac{1}{1-f} = \frac{1}{\log\chi}\,\frac{1}{1 - S^*/\log\chi} = \frac{1}{\log\chi - S^*} = \frac{1}{\xi^*} = 36, \tag{105}$$

the geometric sum read as the layer-by-layer accumulation of the source at the inverse capacity $1/\log\chi$, each layer carrying the fraction f of the last. The descent suppression is $\exp(-S_{\text{eff}}) = \exp(-1/\xi^*) = 2.31952\times10^{-16}$.

9.2 Colour representation

The Higgs field and the colour flux sit on the two sides of the colour decomposition

$$\mathbf{3}\otimes\bar{\mathbf{3}} = \mathbf{8}\oplus\mathbf{1}, \tag{106}$$

the product of the fundamental and its conjugate splitting into the eight-dimensional adjoint and the one-dimensional singlet, with $3\times3 = 9 = 8+1$. The colour representation factor Θ is the colour charge the object carries over the channels it propagates through, the trace of the identity on the charge over the trace of the identity on the channels,

$$\Theta = \frac{\mathrm{Tr}_{\text{charge}}(\mathbb{1})}{\mathrm{Tr}_{\text{channel}}(\mathbb{1})}. \tag{107}$$

The Higgs field is colourless. The charge it carries is the singlet, so the numerator is $\mathrm{Tr}_{\text{charge}}(\nVdash) = 1$; the channel it propagates through is the singlet, so the denominator is $\mathrm{Tr}_{\text{channel}}(\nVdash) = 1$,

$$\Theta_\psi = \frac{\mathrm{Tr}_{\text{charge}}(\nVdash)}{\mathrm{Tr}_{\text{channel}}(\nVdash)} = \frac{1}{1} = 1. \tag{108}$$

The colour flux carries fundamental colour charge, the source it emanates from, so the numerator is $\mathrm{Tr}_{\text{charge}}(\nVdash) = 3$; the channels it propagates through are the adjoint of (106), the eight gluons it is built from, so the denominator is $\mathrm{Tr}_{\text{channel}}(\nVdash) = 8$,

$$\Theta_{b_s} = \frac{\mathrm{Tr}_{\text{charge}}(\nVdash)}{\mathrm{Tr}_{\text{channel}}(\nVdash)} = \frac{3}{8}. \tag{109}$$

Both factors read off the one decomposition (106), the numerator the colour charge the object carries, the singlet 1 or the fundamental 3, and the denominator the channels it propagates through, the singlet 1 or the adjoint 8.

9.3 Spectrum

The spectral weight is the mode's propagator weight against the whole trace of its operator. Let M be either prism operator, with eigenvalues $\lambda_n + 1$ and orthonormal eigenvectors $|n\rangle$, $M^{-1} = \sum_n |n\rangle\langle n|/(\lambda_n + 1)$. A mode ϕ expanded in the eigenbasis, $|\phi\rangle = \sum_n c_n |n\rangle$ with $c_n = \langle n|\phi\rangle$, has propagator weight

$$G_\phi = \frac{\langle\phi|M^{-1}|\phi\rangle}{\langle\phi|\phi\rangle} = \frac{1}{|\phi|^2}\sum_n \frac{c_n^2}{\lambda_n + 1} = \sum_\lambda \frac{\widehat{c}_\lambda^2}{\lambda + 1}, \qquad \widehat{c}_\lambda^2 = \frac{\|P_\lambda\phi\|^2}{|\phi|^2}, \tag{110}$$

$P_\lambda = \sum_{n:\lambda_n=\lambda} |n\rangle\langle n|$ the projector onto the eigenspace of λ. The spectral weight is this propagator weight over the trace of the same operator,

$$\Pi = \frac{G_\phi}{\mathrm{Tr}\, M^{-1}} = \frac{\displaystyle\sum_\lambda \frac{\widehat{c}_\lambda^2}{\lambda + 1}}{\displaystyle\sum_\lambda \frac{m_\lambda}{\lambda + 1}}. \tag{111}$$

The exponent p counts the field factors, one for a scalar field and two for the square of a vector field. The colour representation factor Θ and the spectral weight Π enter the master equation (102) as the product $\Theta\Pi^p$.

10 The electroweak vacuum expectation value

The Higgs field is a scalar mode of the vertex operator. The vacuum expectation value is its spectral weight in the trace of the vertex operator, at the first power for the scalar and weighted by the singlet representation factor of the colourless mode.

The vacuum leaves the spatial cube unbroken, so the Higgs mode is invariant under $\mathrm{Aut}(Q_3)$, acting on x, y, z with τ fixed. $\mathrm{Aut}(Q_3)$ is transitive on the vertices of each cube slice, so of the sixteen vertex modes an invariant one is constant on each slice, a function of τ alone; on the two slices these are the constant $\mathbf{1}$ at $\lambda = 0$ and the alternating $(-1)^\tau$ at $\lambda = 2$. The constant lies in the kernel of the coboundary, $d_0\mathbf{1} = 0$, with no edge content and no contour, and carries no vacuum expectation value; the alternating mode has $d_0\psi \neq 0$ on every temporal edge. The Higgs field is the temporal mode.

The scalar mode is the temporal mode of the vertex operator, the alternating function on the temporal direction and constant on the three cube directions,

$$\psi(x, y, z, \tau) = (-1)^\tau, \tag{112}$$

a one on the eight vertices with $\tau = 0$ and a minus one on the eight vertices with $\tau = 1$, so $|\psi|^2 = \sum_v \psi(v)^2 = 16$. It is the product of the constant vector on each cube factor and the alternating vector on the temporal factor. The vertex operator is the Cartesian sum over the four factors, and on a product mode its eigenvalue is the sum of the factor eigenvalues, zero on each constant cube factor and two on the alternating temporal factor,

$$L_0\psi = (0+0+0+2)\,\psi = 2\,\psi, \qquad \lambda_\psi = 2. \tag{113}$$

The mode is a single eigenvector of L_0. Its projection weights onto the eigenspaces of M_0, from $\|P_\lambda\,\psi\|^2 = \langle\psi|P_\lambda|\psi\rangle$, are concentrated in the one eigenspace,

$$\|P_0\psi\|^2 = 0, \quad \|P_2\psi\|^2 = 16, \quad \|P_4\psi\|^2 = 0, \quad \|P_6\psi\|^2 = 0, \quad \|P_8\psi\|^2 = 0, \tag{114}$$

which sum to $16 = |\psi|^2$, so the normalized weights $\widehat{c}^2_\lambda = \|P_\lambda\,\psi\|^2/16$ are $0,1,0,0,0$, a single surviving weight at $\lambda_\psi = 2$.

The temporal mode is flat across the disentangler plane. The disentangler weight introduced in §8 acts only on the (x,y) edges, and ψ depends only on τ, so the deformation leaves it untouched and its eigenvalue is unchanged from the bare to the deformed operator,

$$L_\omega\psi = L_0\psi = 2\,\psi, \tag{115}$$

leaving $\lambda_\psi = 2$ in both spectra. From (110) the propagator weight is the sum over the spectrum, and with one surviving normalized weight the single term remains,

$$G_\psi = \sum_\lambda \frac{\widehat{c}^2_\lambda}{\lambda+1} = \frac{1}{2+1} = \frac{1}{3}, \tag{116}$$

and the denominator is the vertex Sakharov trace, the deformed trace that closes G_N in §8, the same trace of the same vertex operator, summed over the deformed vertex spectrum,

$$\begin{aligned}\Sigma_V = \mathrm{Tr}\,M_\omega^{-1} = \sum_n \frac{1}{\lambda_n+1} &= \frac{1}{1} + \frac{2}{3} + \frac{2}{3.7857} + \frac{1}{5} + \frac{4}{5.7857} \\ &\quad + \frac{1}{6.5713} + \frac{2}{7.7857} + \frac{2}{8.5713} + \frac{1}{10.5713} = 3.82333,\end{aligned} \tag{117}$$

the nine deformed eigenvalues of (96) with their multiplicities, so the spectral weight is

$$\Pi_\psi = \frac{G_\psi}{\Sigma_V} = \frac{1/3}{3.82333} = 0.087184. \tag{118}$$

The mode is a scalar, the dimension-one scalar $\langle\psi\rangle$, so the spectral weight enters at the first power, $p = 1$.

The mode is a colour singlet, so its representation factor is the singlet value $\Theta_\psi = 1$ of (108). From the master equation (102), with the spectral weight at the first power and the singlet representation factor,

$$v = m_P\,\Theta_\psi\,\Pi_\psi\,\exp(-1/\xi^*), \tag{119}$$

and substituting,

$$v = 1.2209 \times 10^{19}\ \mathrm{GeV} \cdot 1 \cdot 0.087184 \cdot 2.31952 \times 10^{-16} = 246.9\ \mathrm{GeV}, \tag{120}$$

within 0.28% of the measured value (246.22 GeV) [13]. The temporal mode as one component of the electroweak Higgs multiplet, its custodial structure, quantum numbers, and quartic are developed in the companion document `higgs_multiplet_extras`.

11 The string tension

The string tension is the strong counterpart of the vacuum expectation value. Where the Higgs field is a scalar mode of the vertex operator and carries the vertex Sakharov trace at the first power, the colour flux is a vector on the edges, and the string tension carries the edge Sakharov trace squared and weighted by the fundamental representation factor of the colour flux.

The colour flux is a vector on the colour edges. On the cube the colour contour lives on the four z-edges, and each of the eight vertices lies on one z-edge, the edge flipping its z bit. The closure condition at a vertex is the signed sum of the flux over the edges meeting it, and with one z-edge per vertex this is a single term,

$$(d_0^{\mathsf{T}} b_s)_v = \pm b_s(e_v) = 0 \quad \Rightarrow \quad b_s(e_v) = 0, \tag{121}$$

one equation per vertex setting every z-edge coefficient to zero, so $b_s = 0$ on the cube and there is no confining contour (§3). The colour edges are the z-edges, and the only direction the prism adds is τ, so the face that can carry the colour flux is the $z\tau$-face, which does not exist on the cube. On the face at $(x,y) = (0,0)$, with z-edges $(0000)-(0010)$, $(0001)-(0011)$ and τ-edges $(0000)-(0001)$, $(0010)-(0011)$, the flux is the $z\tau$ component of the field strength, one z index and one τ index, odd under the z-reflection $z \mapsto 1-z$ of the face and odd under the τ-reflection $\tau \mapsto 1-\tau$. On the four edges of the face this parity class is exactly two-dimensional and splits orthogonally into its closed part, the circulation around the face, and its sourced part, the alternating vector. The confining string is sourced, a quark at one end and an antiquark at the other; the circulation carries zero boundary and no charges. The flux is the sourced part, unique up to normalization,

$$\begin{aligned} b_s\big((0000)-(0010)\big) &= +1, \quad b_s\big((0010)-(0011)\big) = -1, \\ b_s\big((0001)-(0011)\big) &= -1, \quad b_s\big((0000)-(0001)\big) = +1, \end{aligned} \tag{122}$$

with $|b_s|^2 = 4$, the normalization cancelling in the weights of (110). Its boundary, $(d_0^{\mathsf{T}} b_s)_v = -2, +2, +2, -2$ at the four face vertices, is the source pattern of the string. The colour flux is zero on the cube and nonzero on the prism, so the string tension is a prism quantity, as gravity is.

Let $M_1 = L_1 + I$ be the edge operator, with eigenvalues $\lambda_n + 1$ and orthonormal eigenvectors $|n\rangle$, $L_1|n\rangle = \lambda_n|n\rangle$. The inverse has the spectral resolution $M_1^{-1} = \sum_n |n\rangle\langle n|/(\lambda_n+1)$. The flux b_s is the field strength $F_{z\tau}$; it is not a single eigenvector of M_1, so it spreads over the edge spectrum. The projector onto the eigenspace of L_1 with eigenvalue λ is the sum over its orthonormal eigenvectors, and the squared norm of the projection of b_s into that eigenspace is

$$\|P_\lambda b_s\|^2 = \langle b_s|P_\lambda|b_s\rangle = \sum_{n:\,\lambda_n=\lambda} |\langle n|b_s\rangle|^2. \tag{123}$$

Evaluating on the flux b_s for each eigenvalue of L_1,

$$\|P_0 b_s\|^2 = \frac{7}{6}, \quad \|P_2 b_s\|^2 = 0, \quad \|P_4 b_s\|^2 = 1, \quad \|P_6 b_s\|^2 = \frac{4}{3}, \quad \|P_8 b_s\|^2 = \frac{1}{2}, \tag{124}$$

summing to $\frac{7}{6} + 0 + 1 + \frac{4}{3} + \frac{1}{2} = 4 = |b_s|^2$, so the normalized weights $\widehat{c}_\lambda^2 = \|P_\lambda b_s\|^2/4$ are

$$\widehat{c}_0^2 = \frac{7/6}{4} = \frac{7}{24}, \quad \widehat{c}_2^2 = 0, \quad \widehat{c}_4^2 = \frac{1}{4}, \quad \widehat{c}_6^2 = \frac{4/3}{4} = \frac{1}{3}, \quad \widehat{c}_8^2 = \frac{1/2}{4} = \frac{1}{8}, \tag{125}$$

summing to 1. From (110) the propagator weight is the sum over the spectrum,

$$G_{b_s} = \sum_\lambda \frac{\widehat{c}_\lambda^2}{\lambda+1} = \frac{7/24}{0+1} + \frac{0}{2+1} + \frac{1/4}{4+1} + \frac{1/3}{6+1} + \frac{1/8}{8+1} = \frac{7}{24} + \frac{1}{20} + \frac{1}{21} + \frac{1}{72}, \tag{126}$$

and over the common denominator $\operatorname{lcm}(24,20,21,72) = 2520$,

$$G_{b_s} = \frac{735}{2520} + \frac{126}{2520} + \frac{120}{2520} + \frac{35}{2520} = \frac{1016}{2520} = \frac{127}{315} = 0.403175. \tag{127}$$

The denominator is the edge Sakharov trace, the sum over the edge spectrum (71) in the same form as the vertex trace,

$$\Sigma_E = \mathrm{Tr}\, M_1^{-1} = \sum_\lambda \frac{m_\lambda}{\lambda+1} = \frac{17}{1} + \frac{4}{3} + \frac{6}{5} + \frac{4}{7} + \frac{1}{9}, \tag{128}$$

and over the common denominator $\mathrm{lcm}(1,3,5,7,9) = 315$,

$$\Sigma_E = \frac{5355}{315} + \frac{420}{315} + \frac{378}{315} + \frac{180}{315} + \frac{35}{315} = \frac{6368}{315} = 20.21587, \tag{129}$$

the seventeen zero-modes of the edge kernel carrying the leading term. The spectral weight is

$$\Pi_{b_s} = \frac{G_{b_s}}{\Sigma_E} = \frac{127/315}{6368/315} = \frac{127}{6368} = 0.019943. \tag{130}$$

The flux is a vector, so the spectral weight enters squared, $p = 2$.

The flux carries colour. The confining string carries fundamental colour charge and threads the octet of $\mathbf{3} \otimes \bar{\mathbf{3}} = \mathbf{8} \oplus \mathbf{1}$ [18], so its representation factor is the fundamental value $\Theta_{b_s} = 3/8$ of (109). From the master equation (102), with the spectral weight squared and one power of the representation factor,

$$\sqrt{\sigma} = m_P\, \Theta_{b_s}\, \Pi_{b_s}^2 \exp(-1/\xi^*), \tag{131}$$

and substituting,

$$\Theta_{b_s} \Pi_{b_s}^2 = \frac{3}{8}\left(\frac{127}{6368}\right)^2 = \frac{3}{8} \cdot \frac{16129}{40551424} = \frac{48387}{324411392} = 1.49153 \times 10^{-4}, \tag{132}$$

$$\sqrt{\sigma} = 1.2209 \times 10^{19}\ \mathrm{GeV} \cdot 1.49153 \times 10^{-4} \cdot 2.31952 \times 10^{-16} = 422.4\ \mathrm{MeV}, \tag{133}$$

in agreement with the string-tension value $\sigma = 0.18\ \mathrm{GeV}^2$ ($\sqrt{\sigma} = 424.264$ MeV) determined from the hadron spectrum [35].

12 Verification

The verification script builds the graph geometry of Q_3 and Q_4 with NetworkX, constructs each operator, and compares the results against the matrices presented herein. It checks the internal consistency of the construction and is openly available at Zenodo (DOI: 10.5281/zenodo.21404333).

13 Conclusion

Black-hole physics and high-energy particle physics have been brought together at the Planck scale on a single geometry. One MERA over the cube Q_3 and the prism Q_4, with each bond a harmonic oscillator carrying relative entropy bounded by the Bekenstein–Hawking value $\log\chi = S_{\mathrm{BH}}\ell_P^2/A = 1/4$, yields both the gauge sector and the energy scales of the low-energy world.

The gauge couplings arise as information on the cube. The 1+2 anisotropic split makes z isometric and x, y disentanglers, placing $\mathrm{SU}(3)_c$ on the matching bundle, $\mathrm{SU}(2)_L$ on the xy-face loops, and $\mathrm{U}(1)_Y$ on the body diagonal. The deformation coefficients are counts off the entanglement operators, $c_I = 4$ the open star of the z-edge under I_z and $c_C = 2$ the placement count of D_{xy}. The pair places $\sin^2\theta_W$ within 0.025% of the PDG value, in which the strong coupling cancels so the angle is set by the deformation alone. The gravitational constant is the propagator trace of the deformed prism, $G_N = 0.999057\,\ell_P^2$. The energy scales are spectral projections from the same prism, the electroweak vacuum expectation value $v = 246.9$ GeV as the temporal vertex mode and the confining string tension $\sqrt{\sigma} = 422.4$ MeV as the colour flux on the $z\tau$-face, each carried from the Planck scale to the infrared by the descent of depth $1/\xi^* = 36$.

Gauge structure appears as entanglement information, and the energy scales appear as spectral projections, both from one spectral geometry of the vacuum. The residual capacity $\xi^* = 1/36$ that the vacuum leaves below the Bekenstein–Hawking bound is the single number that sets the deformation of the geometry, the gauge couplings, and the descent that sets the scales.

A The Rényi family and the $\alpha \to 1$ limit

The Rényi divergences [29] form a one-parameter family

$$D_\alpha(\rho\|\sigma) = \frac{1}{\alpha-1}\log\mathrm{tr}(\rho^\alpha\sigma^{1-\alpha}), \qquad \alpha>0,\ \alpha\neq 1, \tag{134}$$

that interpolates between distinct information-theoretic measures. Among these, the Umegaki relative entropy D_{KL} of §2.1 is recovered at $\alpha = 1$ as the unique point satisfying all four conditions (1)–(4) stated there.

At $\alpha = 1$ the formula (134) is indeterminate (0/0). The numerator $\log\mathrm{tr}(\rho^\alpha\sigma^{1-\alpha}) \to \log\mathrm{tr}(\rho) = \log 1 = 0$ and the denominator $\alpha - 1 \to 0$. By L'Hôpital's rule,

$$\lim_{\alpha\to 1} D_\alpha(\rho\|\sigma) = \lim_{\alpha\to 1}\frac{d}{d\alpha}\log\mathrm{tr}(\rho^\alpha\sigma^{1-\alpha}). \tag{135}$$

Differentiating the numerator under the trace using $\partial_\alpha(\rho^\alpha\sigma^{1-\alpha}) = \rho^\alpha\sigma^{1-\alpha}(\log\rho - \log\sigma)$,

$$\frac{d}{d\alpha}\log\mathrm{tr}(\rho^\alpha\sigma^{1-\alpha}) = \frac{\mathrm{tr}\big[\rho^\alpha\sigma^{1-\alpha}(\log\rho-\log\sigma)\big]}{\mathrm{tr}(\rho^\alpha\sigma^{1-\alpha})}. \tag{136}$$

At $\alpha = 1$, $\rho^\alpha\sigma^{1-\alpha} = \rho$ and $\mathrm{tr}\,\rho = 1$, so

$$\lim_{\alpha\to 1} D_\alpha(\rho\|\sigma) = \mathrm{tr}\big[\rho(\log\rho - \log\sigma)\big] = D_{\mathrm{KL}}(\rho\|\sigma). \tag{137}$$

The Umegaki relative entropy is the L'Hôpital limit of the Rényi family at $\alpha = 1$.

Why $\alpha = 1$ is privileged. The first-law condition (2) uses the identity $\mathrm{tr}[\rho\,\delta\log\rho] = 0$, which depends on ρ entering linearly under the trace after the variation. For $\alpha \neq 1$,

$$\delta D_\alpha = \frac{\alpha}{1-\alpha}\cdot\frac{\mathrm{tr}[\rho^{\alpha-1}\sigma^{1-\alpha}\,\delta\rho]}{\mathrm{tr}(\rho^\alpha\sigma^{1-\alpha})}, \tag{138}$$

which involves the operator $\rho^{\alpha-1}\sigma^{1-\alpha}$. There is no value of $\alpha \neq 1$ for which δD_α takes the form $\delta\langle K\rangle - \delta S$, so the first law selects $\alpha = 1$ uniquely. Conditions (3) and (4) reinforce. The Ryu–Takayanagi formula relates δS to area with a Bisognano–Wichmann-mediated bridge requiring $K = -\log\sigma$, which enters only at $\alpha = 1$; and the Bekenstein–Hawking bound, a capacity imposed on the dynamical coordinate $D_{\mathrm{KL}}(\rho\|\rho^0)$, takes its scale from the static identity $D_1(\rho\|\sigma^0) = \log\chi - S(\rho)$, which holds only at $\alpha = 1$. Thus D_{KL} is the unique element of the Rényi family at the L'Hôpital limit $\alpha = 1$ and the unique measure satisfying (1)–(4); the two characterisations agree.

A.1 Other measures and conditions (1)–(4)

Von Neumann entropy $S(\rho) = -\mathrm{tr}[\rho\log\rho]$. A candidate bond coordinate must vanish at the reference state σ^0. At the bond reference σ^0_{ij}, the flat state whose eigenvalues are all equal to $e^{-\log\chi}$, $S(\sigma^0) = -\mathrm{tr}[\sigma^0\log\sigma^0] = -\sum e^{-\log\chi}\log e^{-\log\chi} = \log\chi$, the entropy of the maximally mixed state, which is nonzero, violating (1). Moreover S depends only on ρ, no reference σ enters, so the first-law structure with $K = -\log\sigma$ cannot apply. There is no K to vary against, and the Iyer–Wald chain isolating the geometric content of (3) requires the modular subtraction $\langle K\rangle - S$ to drop the bulk-matter term. Without K, that chain fails.

Mutual information $I(A:B) = S(A) + S(B) - S(AB)$. $I(A:B)$ vanishes on product states $\rho_{AB} = \rho_A\otimes\rho_B$ and only there. The MERA vacuum is entangled across any bisection $A|B$, so $I(A:B) > 0$ at the reference state, violating (1). For (2), the first law requires a single modular Hamiltonian; mutual information involves three (K_A, K_B, K_{AB}) with $\delta I = \delta\langle K_{AB}\rangle - \delta\langle K_A\rangle - \delta\langle K_B\rangle$, which cannot be written as $\delta\langle K\rangle$ for any single K. (2) fails.

Trace distance, fidelity, Bures. For the trace distance $T(\rho,\sigma)=\frac{1}{2}\|\rho-\sigma\|_1$, $\delta T=\frac{1}{2}\operatorname{tr}[\operatorname{sgn}(\rho-\sigma)\,\delta\rho]$, and $\operatorname{sgn}(\rho-\sigma)$ has eigenvalues ± 1, not $-\log\lambda_i(\sigma)$, so it is not a modular Hamiltonian and no thermodynamic form $\delta\langle K\rangle$ holds. The fidelity $F(\rho,\sigma)=(\operatorname{tr}\sqrt{\sqrt{\sigma}\rho\sqrt{\sigma}})^2$ and Bures distance have variations built from $\sqrt{\sigma}\rho\sqrt{\sigma}$, structurally disconnected from $\log\sigma$; the same (2) obstruction applies.

Quantum Fisher information F_Q. With L_θ the symmetric logarithmic derivative ($\partial_\theta\rho_\theta=\frac{1}{2}\{\rho_\theta,L_\theta\}$), for a perturbation toward a pure state $\rho_\theta=(1-\theta)|\psi\rangle\langle\psi|+\theta\,\tau$ the SLD has eigenvalues $\propto 1/\theta$ on the $|\psi\rangle\langle\psi|$ support, so $F_Q(\theta)\to\infty$ as $\theta\to 0^+$. The Fisher information scales with the inverse purity gap, not with $\log\chi$; no χ-dependent upper bound exists, so (4) is violated.

Rényi entropy $S_\alpha(\rho)=\frac{1}{1-\alpha}\log\operatorname{tr}(\rho^\alpha)$ for $\alpha\neq 1$. At the flat reference σ^0, with all eigenvalues $e^{-\log\chi}$, $S_\alpha(\sigma^0)=\frac{1}{1-\alpha}\log\operatorname{tr}(\sigma^{0\,\alpha})=\frac{1}{1-\alpha}\log e^{-(\alpha-1)\log\chi}=\log\chi$, non-zero for every α, violating (1). For (2), $\delta S_\alpha=\frac{\alpha}{1-\alpha}\operatorname{tr}[\rho^{\alpha-1}\delta\rho]/\operatorname{tr}(\rho^\alpha)$ involves $\rho^{\alpha-1}$; only at $\alpha=1$ does $\rho^{\alpha-1}\to\mathbb{I}$ and the first-law form recover. For (3), the Lewkowycz–Maldacena replica derivation [30] gives a holographic dual with a cosmic brane of tension $T_n=(n-1)/(4nG_N)$; the area-only relation recovers only in the $\alpha\to 1$ tensionless limit.

B Vertex and edge labeling of Q_3

This appendix gives the vertex and edge labeling of Q_3 used by the incidence vectors of §3.5–3.6.

Vertex and edge ordering. Label the eight vertices of Q_3 by binary $(x,y,z)\in\{0,1\}^3$, identified with integers 0–7 by $v=4x+2y+z$. The twelve edges, ordered lexicographically by vertex pairs (i,j) with $i<j$, are:

$$\begin{array}{lll}
e_0:(000)\to(001) & e_1:(000)\to(010) & e_2:(000)\to(100)\\
e_3:(001)\to(011) & e_4:(001)\to(101) & e_5:(010)\to(011)\\
e_6:(010)\to(110) & e_7:(011)\to(111) & e_8:(100)\to(101)\\
e_9:(100)\to(110) & e_{10}:(101)\to(111) & e_{11}:(110)\to(111)
\end{array}$$

B.1 The matching bundle E_z and its incidence matrix

The $SU(3)_c$ strong sector (§3.4) is supported on the matching bundle E_z, the four z-edges of Q_3 oriented from each $z=0$ endpoint to its $z=1$ endpoint:

$$E_z=\{e_0,e_5,e_8,e_{11}\},\qquad \begin{array}{ll} e_0:(000)\to(001), & e_5:(010)\to(011),\\ e_8:(100)\to(101), & e_{11}:(110)\to(111).\end{array} \tag{139}$$

Writing v_i^- and v_i^+ for the $z=0$ and $z=1$ endpoints of the i-th edge of E_z, the net flow of the strong contour b_s of (39) is

$$\partial_1 b_s=\sum_{i=1}^{4}c_i\bigl(v_i^+-v_i^-\bigr). \tag{140}$$

Ordering the eight rows by vertex $(000),(001),(010),(011),(100),(101),(110),(111)$, this is the incidence matrix $B_z=\partial_1\big|_{E_z}\in\{-1,0,+1\}^{8\times 4}$,

$$B_z=\begin{pmatrix}-1&0&0&0\\+1&0&0&0\\0&-1&0&0\\0&+1&0&0\\0&0&-1&0\\0&0&+1&0\\0&0&0&-1\\0&0&0&+1\end{pmatrix},\qquad \partial_1 b_s=B_z c, \tag{141}$$

where $c = (c_1, c_2, c_3, c_4)^\top$ is the strong contour b_s expressed on E_z: its four entries are the signed weights c_i of (39), and the eight components of b_s off the z-edges are zero. Because every vertex of Q_3 lies on one z-edge, each row of B_z carries a single nonzero entry. The closure condition $B_z c = 0$ is therefore eight one-term equations, one per vertex:

$$\begin{aligned} (000):\ -c_1 = 0, \quad (001):\ +c_1 = 0, \\ (010):\ -c_2 = 0, \quad (011):\ +c_2 = 0, \\ (100):\ -c_3 = 0, \quad (101):\ +c_3 = 0, \\ (110):\ -c_4 = 0, \quad (111):\ +c_4 = 0. \end{aligned} \tag{142}$$

Each equation sets one coefficient to zero, recovering $c_1 = c_2 = c_3 = c_4 = 0$ and the vanishing of the strong contour $b_s = 0$ used in §3.4.

C The disentangler and composite operators and their Wilson moments

This appendix packages the explicit calculation of the Wilson moments used for the placement-weighted in-plane disentangler operator D_{xy}, the z-isometry operator I_z, and the disentangler–isometry composite

$$C = \{D_{xy}, I_z\} = D_{xy}I_z + I_z D_{xy}. \tag{143}$$

D_{xy} is a *placement-weighted* operator: different MERA placements that write the same unordered edge pair add their weights. Thus the four diagonal placements write sixteen pair contributions in all, although these reduce to twelve distinct unordered pairs after duplicate pairs are forgotten.

Value	Moment	Interpretation
-8	$b_L^\top D_{xy} b_L$	Direct in-plane disentangler moment in the $\mathrm{SU}(2)_L$ loop.
$\frac{3}{2}$	$(b_Y)^\top D_{xy} b_Y$	Direct in-plane disentangler moment in the $\mathrm{U}(1)_Y$ line. The two in-plane staircase edges e_2, e_9 share a vertex and are connected by D_{xy}, weighted by $(\sqrt{3}/2)^2 = \frac{3}{4}$.
0	$b_L^\top I_z b_L$	Pure z-isometry moment in the $\mathrm{SU}(2)_L$ loop. The weak loop has no z-edge support.
$\frac{3}{2}$	$(b_Y)^\top I_z b_Y$	Pure z-isometry moment in the $\mathrm{U}(1)_Y$ line. The z staircase edge e_{11} is joined by I_z to the in-plane edges at its endpoints, weighted by $\frac{3}{4}$.
0	$b_L^\top C b_L$	Composite disentangler–isometry moment in the $\mathrm{SU}(2)_L$ loop. The composite has in-plane–z support and therefore does not close on the weak loop.
6	$(b_Y)^\top C b_Y$	Composite disentangler–isometry moment in the $\mathrm{U}(1)_Y$ line, weighted by $\frac{3}{4}$.

Table 6: Complete six-moment accounting. The compressed list is $-8, \frac{3}{2}, 0, \frac{3}{2}, 0, 6$, ordered as $(D_L, D_Y, I_L, I_Y, C_L, C_Y)$.

Incidence vectors. All vectors are written in the edge basis $(e_0, \ldots, e_{11})$ of Appendix B. The weak face-loop vector b_L is supported on the $z = 0$ face:

$$\begin{aligned} b_L = (0, -1, +1, 0, 0, 0, -1, 0, 0, +1, 0, 0)^\top, \\ \text{i.e.}\quad b_L(e_1) = -1,\ b_L(e_2) = +1,\ b_L(e_6) = -1,\ b_L(e_9) = +1, \end{aligned} \tag{144}$$

and all other components vanish. The hypercharge vector b_Y is the staircase representation of the body diagonal, carrying the circumradius weight $\sqrt{3}/2$,

$$b_Y = \frac{\sqrt{3}}{2}(0,0,1,0,0,0,0,0,0,1,0,1)^\top, \quad \text{so} \quad b_Y(e_2) = b_Y(e_9) = b_Y(e_{11}) = \frac{\sqrt{3}}{2}, \tag{145}$$

and all other components vanish. For any real-symmetric operator O with vanishing diagonal,

$$b^\top O b = \sum_{a<c} 2 O_{ac} b_a b_c. \tag{146}$$

This is the contraction rule used throughout the calculation.

The placement-weighted disentangler D_{xy}. The in-plane disentanglers sit on the two diagonals of each xy face. Each diagonal placement writes four cross-correlations among the four in-face edges: two share-vertex pairs and two parallel opposite-edge pairs. On a single face, the two diagonal placements write the four share-vertex pairs once each, while the two parallel pairs are written by both diagonals and therefore carry weight 2. On the $z=0$ face, with in-plane edges e_1, e_2, e_6, e_9, the nonzero entries of D_{xy} are

$$\begin{aligned} \text{share-vertex pairs, weight 1}: &\quad (e_1,e_2),\ (e_1,e_6),\ (e_2,e_9),\ (e_6,e_9), \\ \text{parallel pairs, weight 2}: &\quad (e_2,e_6),\ (e_1,e_9). \end{aligned} \tag{147}$$

On the $z=1$ face, with in-plane edges e_3, e_4, e_7, e_{10}, the corresponding entries are

$$\begin{aligned} \text{share-vertex pairs, weight 1}: &\quad (e_3,e_4),\ (e_3,e_7),\ (e_4,e_{10}),\ (e_7,e_{10}), \\ \text{parallel pairs, weight 2}: &\quad (e_4,e_7),\ (e_3,e_{10}). \end{aligned} \tag{148}$$

The matrix is symmetric and has zero diagonal. Equations (147) and (148) define all nonzero entries of D_{xy}.

Weak moment of D_{xy}. This accounts for the first entry of Table 6, namely the value -8. Only the $z=0$ face contributes to $b_L^\top D_{xy} b_L$. Using (146), the share-vertex contribution is

$$\begin{aligned} &2(1)b_L(e_1)b_L(e_2) + 2(1)b_L(e_1)b_L(e_6) + 2(1)b_L(e_2)b_L(e_9) + 2(1)b_L(e_6)b_L(e_9) \\ &= 2(-1)(+1) + 2(-1)(-1) + 2(+1)(+1) + 2(-1)(+1) = -2+2+2-2 = 0. \end{aligned} \tag{149}$$

The parallel contribution is

$$2(2)b_L(e_2)b_L(e_6) + 2(2)b_L(e_1)b_L(e_9) = 2\cdot 2(+1)(-1) + 2\cdot 2(-1)(+1) = -4-4 = -8. \tag{150}$$

Therefore $b_L^\top D_{xy} b_L = -8$. The share-vertex pairs cancel by sign. The full weak moment comes from the two placement-weighted parallel pairs.

Hypercharge moment of D_{xy}. This accounts for the second entry of Table 6. The staircase $b_Y = \frac{\sqrt{3}}{2}(e_2 + e_9 + e_{11})$ has two in-plane edges e_2, e_9 and one z-edge e_{11}. The in-plane disentangler connects the two in-plane edges, which share the vertex (100),

$$(D_{xy})_{e_2 e_9} = 1, \tag{151}$$

and has no entry touching the z-edge e_{11}. With the circumradius weight $(\sqrt{3}/2)^2 = \frac{3}{4}$, $(b_Y)^\top D_{xy} b_Y = \frac{3}{4}\cdot 2(D_{xy})_{e_2 e_9} = \frac{3}{4}\cdot 2 = \frac{3}{2}$.

The isometry I_z. The operator I_z correlates each z-edge with the in-plane bonds incident to its two endpoints. Thus I_z has only in-plane–z entries and no in-plane–in-plane or z–z entries. The entries relevant for the hypercharge calculation are

$$(I_z)_{e_6e_{11}} = (I_z)_{e_9e_{11}} = (I_z)_{e_7e_{11}} = (I_z)_{e_{10}e_{11}} = 1, \tag{152}$$

with symmetry giving the reversed entries. The next two contractions account for the third and fourth entries of Table 6. Since b_L has no support on any z-edge, and since I_z contains only in-plane–z entries, $b_L^\top I_z b_L = 0$. For b_Y, the staircase z-edge e_{11} is joined by I_z to the in-plane staircase edge e_9, which meets it at the vertex (110), $(I_z)_{e_9e_{11}} = 1$, so with the weight $\frac{3}{4}$, $(b_Y)^\top I_z b_Y = \frac{3}{4}\cdot 2(I_z)_{e_9e_{11}} = \frac{3}{4}\cdot 2 = \frac{3}{2}$.

The composite $C = \{D_{xy}, I_z\}$. Because D_{xy} is in-plane–in-plane and I_z is in-plane–z, the composite has in-plane–z support. Therefore it does not connect two weak-loop edges, since b_L has support only on in-plane edges. This vanishing contraction is the fifth entry of Table 6, so $b_L^\top C b_L = 0$. For the hypercharge staircase, the composite connects the z-edge e_{11} to the in-plane staircase edges e_2 and e_9 through $C_{e_2e_{11}}$ and $C_{e_9e_{11}}$. The term I_zD_{xy} cannot contribute, because it would require D_{xy} to act on the z-edge e_{11}, which it does not do, hence $C_{e_2e_{11}} = \sum_k (D_{xy})_{e_2k}(I_z)_{ke_{11}}$. The only intermediate in-plane edges k that connect to e_2 through D_{xy} and to e_{11} through I_z are e_6 and e_9, so

$$C_{e_2e_{11}} = (D_{xy})_{e_2e_6}(I_z)_{e_6e_{11}} + (D_{xy})_{e_2e_9}(I_z)_{e_9e_{11}} = 2\cdot 1 + 1\cdot 1 = 3, \tag{153}$$

and for the e_9–e_{11} pair the only intermediate edge is e_6, $C_{e_9e_{11}} = (D_{xy})_{e_9e_6}(I_z)_{e_6e_{11}} = 1\cdot 1 = 1$. With the circumradius weight $\frac{3}{4}$, $(b_Y)^\top C b_Y = \frac{3}{4}\cdot 2\left(C_{e_2e_{11}} + C_{e_9e_{11}}\right) = \frac{3}{4}\cdot 2(3+1) = 6$.

Moment summary and accounting. The complete set of moments is therefore

Incidence vector	D_{xy}	I_z	$C = \{D_{xy}, I_z\}$
b_L	-8	0	0
b_Y	$\frac{3}{2}$	$\frac{3}{2}$	6

Table 7: Full six-entry moment accounting for the two Wilson contours and the three operators. The six displayed entries are ordered as $(D_L, D_Y, I_L, I_Y, C_L, C_Y) = (-8, \frac{3}{2}, 0, \frac{3}{2}, 0, 6)$.

Placement multiplicity check. The value -8 for the weak moment depends on keeping MERA placement multiplicity. On each xy face, the two diagonal disentangler placements write the same two parallel edge pairs. With multiplicity, those two pairs have weight 2, giving

$$2\cdot 2(+1)(-1) + 2\cdot 2(-1)(+1) = -8. \tag{154}$$

If the duplicate placements were discarded and D_{xy} were replaced by a deduplicated pair-union operator, the parallel weights would be 1 instead of 2, and the weak moment would become

$$2\cdot 1(+1)(-1) + 2\cdot 1(-1)(+1) = -4. \tag{155}$$

Thus the manuscript moments use the placement-weighted operator, not the deduplicated pair-union operator. The accounting in Tables 6 and 7 also shows the sector structure. The weak loop lies entirely in the disentangler plane, so it is moved by D_{xy} and untouched by I_z and C. The hypercharge staircase crosses all three axes, so it couples to all three operators, the in-plane segments through D_{xy}, the z segment through I_z, and the transfer across the layer through C. This is the operator-level origin of the moment pattern

$$\mathrm{SU}(2)_L:\ -8, \qquad \mathrm{U}(1)_Y:\ \left(\tfrac{3}{2}, \tfrac{3}{2}, 6\right), \tag{156}$$

the weak loop confined to the disentangler channel and the hypercharge line spread across all three.

Explicit block matrices. The block basis is

$$(E_{xy}, E_z) = (e_1, e_2, e_3, e_4, e_6, e_7, e_9, e_{10}; e_0, e_5, e_8, e_{11}). \tag{157}$$

The 8×8 in-plane disentangler block D, with share-vertex entries 1 and placement-weighted parallel entries 2, is

$$D = \begin{pmatrix} 0 & 1 & 0 & 0 & 1 & 0 & 2 & 0 \\ 1 & 0 & 0 & 0 & 2 & 0 & 1 & 0 \\ 0 & 0 & 0 & 1 & 0 & 1 & 0 & 2 \\ 0 & 0 & 1 & 0 & 0 & 2 & 0 & 1 \\ 1 & 2 & 0 & 0 & 0 & 0 & 1 & 0 \\ 0 & 0 & 1 & 2 & 0 & 0 & 0 & 1 \\ 2 & 1 & 0 & 0 & 1 & 0 & 0 & 0 \\ 0 & 0 & 2 & 1 & 0 & 1 & 0 & 0 \end{pmatrix}. \tag{158}$$

The 8×4 isometric incidence block B joins each z-edge to the in-plane edges meeting it,

$$B = \begin{pmatrix} 1 & 1 & 0 & 0 \\ 1 & 0 & 1 & 0 \\ 1 & 1 & 0 & 0 \\ 1 & 0 & 1 & 0 \\ 0 & 1 & 0 & 1 \\ 0 & 1 & 0 & 1 \\ 0 & 0 & 1 & 1 \\ 0 & 0 & 1 & 1 \end{pmatrix}, \qquad I_z = \begin{pmatrix} 0_{8\times 8} & B \\ B^{\top} & 0_{4\times 4} \end{pmatrix}. \tag{159}$$

The composite $C = \{D_{xy}, I_z\}$ has off-diagonal blocks DB and $B^{\top}D$,

$$DB = \begin{pmatrix} 1 & 1 & 3 & 3 \\ 1 & 3 & 1 & 3 \\ 1 & 1 & 3 & 3 \\ 1 & 3 & 1 & 3 \\ 3 & 1 & 3 & 1 \\ 3 & 1 & 3 & 1 \\ 3 & 3 & 1 & 1 \\ 3 & 3 & 1 & 1 \end{pmatrix}, \qquad C = \begin{pmatrix} 0_{8\times 8} & DB \\ B^{\top}D & 0_{4\times 4} \end{pmatrix}. \tag{160}$$

On the prism Q_4, the direct disentangler $D_{xy}^{(Q_4)}$ is the 32×32 edge operator built by the same rule as on the cube. On each xy-face (a face fixing both z and the temporal coordinate τ) the two diagonal placements write the four share-vertex pairs once each (weight 1) and the two parallel opposite-edge pairs with weight 2, with entries $\{1,2\}$ and zero diagonal. There are 16 in-plane (x,y) edges and 16 z/temporal edges. Its row-sum vector $\mathbf{r} = D_{xy}^{(Q_4)}\mathbf{1}$, indexed by the prism edges in the vertex order $0000, \ldots, 1111$, is

$$\mathbf{r} = (4,4,0,0,4,4,0,4,4,0,4,4,4,0,0,4,0,4,0,4,4,0,0,4,0,4,0,4,0,0,0,0)^{\top}, \tag{161}$$

so the row sum is 4 on every in-plane edge and 0 on the z and temporal edges. The gravitational edge weight $\omega_k = 1 + c_D \big(D_{xy}^{(Q_4)}\mathbf{1}\big)_k = 1 + c_D r_k$ with $c_D = \frac{5}{\sqrt{2}}\,\xi^* = 0.098209$ is therefore

$$\omega_k = 1 + 4\,c_D = 1.3928 \ \ \text{(in-plane edges)}, \qquad \omega_k = 1 \ \ (z \text{ and temporal edges}). \tag{162}$$

D The bond action and its inverse at $(c_I, c_C) = (4,2)$

At coefficients $c_I = 4\,\xi^*$ and $c_C = 2\,\xi^*$, the off-diagonal entries are $32(c_I - c_C) = 1.7778$ and $-32\,c_C \cdot 3 = -5.3333$, displayed to four decimals so the printed operator reproduces its printed inverse. In the same block basis,

$$M_{Q_3}^{(4,2)} = \begin{pmatrix}
32 & 0 & 0 & 0 & 0 & 0 & 0 & 0 & 1.7778 & 1.7778 & -5.3333 & -5.3333 \\
0 & 32 & 0 & 0 & 0 & 0 & 0 & 0 & 1.7778 & -5.3333 & 1.7778 & -5.3333 \\
0 & 0 & 32 & 0 & 0 & 0 & 0 & 0 & 1.7778 & 1.7778 & -5.3333 & -5.3333 \\
0 & 0 & 0 & 32 & 0 & 0 & 0 & 0 & 1.7778 & -5.3333 & 1.7778 & -5.3333 \\
0 & 0 & 0 & 0 & 32 & 0 & 0 & 0 & -5.3333 & 1.7778 & -5.3333 & 1.7778 \\
0 & 0 & 0 & 0 & 0 & 32 & 0 & 0 & -5.3333 & 1.7778 & -5.3333 & 1.7778 \\
0 & 0 & 0 & 0 & 0 & 0 & 32 & 0 & -5.3333 & -5.3333 & 1.7778 & 1.7778 \\
0 & 0 & 0 & 0 & 0 & 0 & 0 & 32 & -5.3333 & -5.3333 & 1.7778 & 1.7778 \\
1.7778 & 1.7778 & 1.7778 & 1.7778 & -5.3333 & -5.3333 & -5.3333 & -5.3333 & 32 & 0 & 0 & 0 \\
1.7778 & -5.3333 & 1.7778 & -5.3333 & 1.7778 & 1.7778 & -5.3333 & -5.3333 & 0 & 32 & 0 & 0 \\
-5.3333 & 1.7778 & -5.3333 & 1.7778 & -5.3333 & -5.3333 & 1.7778 & 1.7778 & 0 & 0 & 32 & 0 \\
-5.3333 & -5.3333 & -5.3333 & -5.3333 & 1.7778 & 1.7778 & 1.7778 & 1.7778 & 0 & 0 & 0 & 32
\end{pmatrix}. \tag{163}$$

The weak 4×4 principal submatrix of $\big(M_{Q_3}^{(4,2)}\big)^{-1}$ on $\{e_1,e_2,e_6,e_9\}$ and the hypercharge 3×3 submatrix on $\{e_2,e_9,e_{11}\}$ are

$$\begin{pmatrix} +0.033601 & +0.000428 & +0.000428 & -0.001495 \\ +0.000428 & +0.033601 & -0.001495 & +0.000428 \\ +0.000428 & -0.001495 & +0.033601 & +0.000428 \\ -0.001495 & +0.000428 & +0.000428 & +0.033601 \end{pmatrix}, \qquad \begin{pmatrix} +0.033601 & +0.000428 & +0.006253 \\ +0.000428 & +0.033601 & -0.002401 \\ +0.006253 & -0.002401 & +0.035952 \end{pmatrix}, \tag{164}$$

giving $\delta_L = 0.070192$ and $\delta_Y = 0.041894$.

E The vertex and edge operators

This appendix writes out the operators of Section 7 in the vertex and edge orderings used throughout. The cube adjacency $A(Q_3)$ and the entanglement matrix M_{ent} drive the eigenvalue scan that selects the MERA. The scalar operator $M_0 = L_0 + I$ carries the gravitational constant through its trace and the electroweak vacuum expectation value through its temporal mode; the edge operator $M_1 = L_1 + I$ carries the string tension through its edge spectrum. The adjacency matrix A and the coboundary d_0 are the building blocks from which L_0 and L_1 are formed. The sixteen vertices are ordered by the binary value of the string (x,y,z,τ), from 0000 to 1111. The thirty-two edges are ordered by tail vertex, then by the flipped bit x,y,z,τ.

The cube adjacency matrix $A(Q_3)$, the eight cube vertices (x,y,z) from 000 to 111 joined when their strings differ in one bit, is

$$A(Q_3) = \begin{bmatrix} 0 & 1 & 1 & 0 & 1 & 0 & 0 & 0 \\ 1 & 0 & 0 & 1 & 0 & 1 & 0 & 0 \\ 1 & 0 & 0 & 1 & 0 & 0 & 1 & 0 \\ 0 & 1 & 1 & 0 & 0 & 0 & 0 & 1 \\ 1 & 0 & 0 & 0 & 0 & 1 & 1 & 0 \\ 0 & 1 & 0 & 0 & 1 & 0 & 0 & 1 \\ 0 & 0 & 1 & 0 & 1 & 0 & 0 & 1 \\ 0 & 0 & 0 & 1 & 0 & 1 & 1 & 0 \end{bmatrix}. \tag{165}$$

Its spectrum is $\{3^{(1)}, 1^{(3)}, -1^{(3)}, -3^{(1)}\}$, and the entanglement matrix $M_{\text{ent}} = \mathbb{I} + (\log\chi)^2 A(Q_3) = \frac{1}{16}\big(16\mathbb{I} + A(Q_3)\big)$ is

$$M_{\text{ent}} = \frac{1}{16}\begin{bmatrix} 16 & 1 & 1 & 0 & 1 & 0 & 0 & 0 \\ 1 & 16 & 0 & 1 & 0 & 1 & 0 & 0 \\ 1 & 0 & 16 & 1 & 0 & 0 & 1 & 0 \\ 0 & 1 & 1 & 16 & 0 & 0 & 0 & 1 \\ 1 & 0 & 0 & 0 & 16 & 1 & 1 & 0 \\ 0 & 1 & 0 & 0 & 1 & 16 & 0 & 1 \\ 0 & 0 & 1 & 0 & 1 & 0 & 16 & 1 \\ 0 & 0 & 0 & 1 & 0 & 1 & 1 & 16 \end{bmatrix}. \tag{166}$$

Its eigenvalues are $\{\frac{19}{16}^{(1)}, \frac{17}{16}^{(3)}, \frac{15}{16}^{(3)}, \frac{13}{16}^{(1)}\}$, the eigenvalue $17/16$ of multiplicity three fixing the central identity.

The vertex adjacency matrix A, two vertices joined when their strings differ in one bit, is

$$A = \begin{bmatrix} 0&1&1&0&1&0&0&0&1&0&0&0&0&0&0&0 \\ 1&0&0&1&0&1&0&0&0&1&0&0&0&0&0&0 \\ 1&0&0&1&0&0&1&0&0&0&1&0&0&0&0&0 \\ 0&1&1&0&0&0&0&1&0&0&0&1&0&0&0&0 \\ 1&0&0&0&0&1&1&0&0&0&0&0&1&0&0&0 \\ 0&1&0&0&1&0&0&1&0&0&0&0&0&1&0&0 \\ 0&0&1&0&1&0&0&1&0&0&0&0&0&0&1&0 \\ 0&0&0&1&0&1&1&0&0&0&0&0&0&0&0&1 \\ 1&0&0&0&0&0&0&0&0&1&1&0&1&0&0&0 \\ 0&1&0&0&0&0&0&0&1&0&0&1&0&1&0&0 \\ 0&0&1&0&0&0&0&0&1&0&0&1&0&0&1&0 \\ 0&0&0&1&0&0&0&0&0&1&1&0&0&0&0&1 \\ 0&0&0&0&1&0&0&0&1&0&0&0&0&1&1&0 \\ 0&0&0&0&0&1&0&0&0&1&0&0&1&0&0&1 \\ 0&0&0&0&0&0&1&0&0&0&1&0&1&0&0&1 \\ 0&0&0&0&0&0&0&1&0&0&0&1&0&1&1&0 \end{bmatrix}. \tag{167}$$

The degree is $D_0 = 4I$, and the vertex Laplacian $L_0 = D_0 - A$ of (65) is

$$L_0 = \begin{bmatrix} 4&-1&-1&0&-1&0&0&0&-1&0&0&0&0&0&0&0 \\ -1&4&0&-1&0&-1&0&0&0&-1&0&0&0&0&0&0 \\ -1&0&4&-1&0&0&-1&0&0&0&-1&0&0&0&0&0 \\ 0&-1&-1&4&0&0&0&-1&0&0&0&-1&0&0&0&0 \\ -1&0&0&0&4&-1&-1&0&0&0&0&0&-1&0&0&0 \\ 0&-1&0&0&-1&4&0&-1&0&0&0&0&0&-1&0&0 \\ 0&0&-1&0&-1&0&4&-1&0&0&0&0&0&0&-1&0 \\ 0&0&0&-1&0&-1&-1&4&0&0&0&0&0&0&0&-1 \\ -1&0&0&0&0&0&0&0&4&-1&-1&0&-1&0&0&0 \\ 0&-1&0&0&0&0&0&0&-1&4&0&-1&0&-1&0&0 \\ 0&0&-1&0&0&0&0&0&-1&0&4&-1&0&0&-1&0 \\ 0&0&0&-1&0&0&0&0&0&-1&-1&4&0&0&0&-1 \\ 0&0&0&0&-1&0&0&0&-1&0&0&0&4&-1&-1&0 \\ 0&0&0&0&0&-1&0&0&0&-1&0&0&-1&4&0&-1 \\ 0&0&0&0&0&0&-1&0&0&0&-1&0&-1&0&4&-1 \\ 0&0&0&0&0&0&0&-1&0&0&0&-1&0&-1&-1&4 \end{bmatrix}. \tag{168}$$

Its spectrum is $\{0^{(1)}, 2^{(4)}, 4^{(6)}, 6^{(4)}, 8^{(1)}\}$ of (68), and the scalar operator is $M_0 = L_0 + I$, whose trace gives the gravitational constant and whose temporal mode $\psi = (-1)^{\tau}$ gives the electroweak vacuum expectation value.

The coboundary d_0 of (69), a 32×16 matrix with $(d_0)_{e,v} = +1$ at the head and -1 at the tail of edge

e, is

$$d_0 = \begin{bmatrix}
-1 & 0 & 0 & 0 & 0 & 0 & 0 & 0 & 1 & 0 & 0 & 0 & 0 & 0 & 0 & 0 \\
-1 & 0 & 0 & 0 & 1 & 0 & 0 & 0 & 0 & 0 & 0 & 0 & 0 & 0 & 0 & 0 \\
-1 & 0 & 1 & 0 & 0 & 0 & 0 & 0 & 0 & 0 & 0 & 0 & 0 & 0 & 0 & 0 \\
-1 & 1 & 0 & 0 & 0 & 0 & 0 & 0 & 0 & 0 & 0 & 0 & 0 & 0 & 0 & 0 \\
0 & -1 & 0 & 0 & 0 & 0 & 0 & 0 & 0 & 1 & 0 & 0 & 0 & 0 & 0 & 0 \\
0 & -1 & 0 & 0 & 0 & 1 & 0 & 0 & 0 & 0 & 0 & 0 & 0 & 0 & 0 & 0 \\
0 & -1 & 0 & 1 & 0 & 0 & 0 & 0 & 0 & 0 & 0 & 0 & 0 & 0 & 0 & 0 \\
0 & 0 & -1 & 0 & 0 & 0 & 0 & 0 & 0 & 0 & 1 & 0 & 0 & 0 & 0 & 0 \\
0 & 0 & -1 & 0 & 0 & 0 & 1 & 0 & 0 & 0 & 0 & 0 & 0 & 0 & 0 & 0 \\
0 & 0 & -1 & 1 & 0 & 0 & 0 & 0 & 0 & 0 & 0 & 0 & 0 & 0 & 0 & 0 \\
0 & 0 & 0 & -1 & 0 & 0 & 0 & 0 & 0 & 0 & 0 & 1 & 0 & 0 & 0 & 0 \\
0 & 0 & 0 & -1 & 0 & 0 & 0 & 1 & 0 & 0 & 0 & 0 & 0 & 0 & 0 & 0 \\
0 & 0 & 0 & 0 & -1 & 0 & 0 & 0 & 0 & 0 & 0 & 0 & 1 & 0 & 0 & 0 \\
0 & 0 & 0 & 0 & -1 & 0 & 1 & 0 & 0 & 0 & 0 & 0 & 0 & 0 & 0 & 0 \\
0 & 0 & 0 & 0 & -1 & 1 & 0 & 0 & 0 & 0 & 0 & 0 & 0 & 0 & 0 & 0 \\
0 & 0 & 0 & 0 & 0 & -1 & 0 & 0 & 0 & 0 & 0 & 0 & 0 & 1 & 0 & 0 \\
0 & 0 & 0 & 0 & 0 & -1 & 0 & 1 & 0 & 0 & 0 & 0 & 0 & 0 & 0 & 0 \\
0 & 0 & 0 & 0 & 0 & 0 & -1 & 0 & 0 & 0 & 0 & 0 & 0 & 0 & 1 & 0 \\
0 & 0 & 0 & 0 & 0 & 0 & -1 & 1 & 0 & 0 & 0 & 0 & 0 & 0 & 0 & 0 \\
0 & 0 & 0 & 0 & 0 & 0 & 0 & -1 & 0 & 0 & 0 & 0 & 0 & 0 & 0 & 1 \\
0 & 0 & 0 & 0 & 0 & 0 & 0 & 0 & -1 & 0 & 0 & 0 & 1 & 0 & 0 & 0 \\
0 & 0 & 0 & 0 & 0 & 0 & 0 & 0 & -1 & 0 & 1 & 0 & 0 & 0 & 0 & 0 \\
0 & 0 & 0 & 0 & 0 & 0 & 0 & 0 & -1 & 1 & 0 & 0 & 0 & 0 & 0 & 0 \\
0 & 0 & 0 & 0 & 0 & 0 & 0 & 0 & 0 & -1 & 0 & 0 & 0 & 1 & 0 & 0 \\
0 & 0 & 0 & 0 & 0 & 0 & 0 & 0 & 0 & -1 & 0 & 1 & 0 & 0 & 0 & 0 \\
0 & 0 & 0 & 0 & 0 & 0 & 0 & 0 & 0 & 0 & -1 & 0 & 0 & 0 & 1 & 0 \\
0 & 0 & 0 & 0 & 0 & 0 & 0 & 0 & 0 & 0 & -1 & 1 & 0 & 0 & 0 & 0 \\
0 & 0 & 0 & 0 & 0 & 0 & 0 & 0 & 0 & 0 & 0 & -1 & 0 & 0 & 0 & 1 \\
0 & 0 & 0 & 0 & 0 & 0 & 0 & 0 & 0 & 0 & 0 & 0 & -1 & 0 & 1 & 0 \\
0 & 0 & 0 & 0 & 0 & 0 & 0 & 0 & 0 & 0 & 0 & 0 & -1 & 1 & 0 & 0 \\
0 & 0 & 0 & 0 & 0 & 0 & 0 & 0 & 0 & 0 & 0 & 0 & 0 & -1 & 0 & 1 \\
0 & 0 & 0 & 0 & 0 & 0 & 0 & 0 & 0 & 0 & 0 & 0 & 0 & 0 & -1 & 1
\end{bmatrix}. \tag{169}$$

The vertex Laplacian factorises as $L_0 = d_0^{\mathsf{T}} d_0$, and the edge Laplacian $L_1 = d_0 d_0^{\mathsf{T}}$ of (70) is the 32×32 operator

$$L_1 = \begin{bmatrix}
2 & 1 & 1 & 1 & 0 & 0 & 0 & 0 & 0 & 0 & 0 & 0 & 0 & 0 & 0 & 0 & 0 & 0 & 0 & 0 & -1 & -1 & -1 & 0 & 0 & 0 & 0 & 0 & 0 & 0 & 0 & 0 \\
1 & 2 & 1 & 1 & 0 & 0 & 0 & 0 & 0 & 0 & 0 & 0 & -1 & -1 & -1 & 0 & 0 & 0 & 0 & 0 & 0 & 0 & 0 & 0 & 0 & 0 & 0 & 0 & 0 & 0 & 0 & 0 \\
1 & 1 & 2 & 1 & 0 & 0 & 0 & -1 & -1 & -1 & 0 & 0 & 0 & 0 & 0 & 0 & 0 & 0 & 0 & 0 & 0 & 0 & 0 & 0 & 0 & 0 & 0 & 0 & 0 & 0 & 0 & 0 \\
1 & 1 & 1 & 2 & -1 & -1 & -1 & 0 & 0 & 0 & 0 & 0 & 0 & 0 & 0 & 0 & 0 & 0 & 0 & 0 & 0 & 0 & 0 & 0 & 0 & 0 & 0 & 0 & 0 & 0 & 0 & 0 \\
0 & 0 & 0 & -1 & 2 & 1 & 1 & 0 & 0 & 0 & 0 & 0 & 0 & 0 & 0 & 0 & 0 & 0 & 0 & 0 & 0 & 0 & 1 & -1 & -1 & 0 & 0 & 0 & 0 & 0 & 0 & 0 \\
0 & 0 & 0 & -1 & 1 & 2 & 1 & 0 & 0 & 0 & 0 & 0 & 0 & 0 & 1 & -1 & -1 & 0 & 0 & 0 & 0 & 0 & 0 & 0 & 0 & 0 & 0 & 0 & 0 & 0 & 0 & 0 \\
0 & 0 & 0 & -1 & 1 & 1 & 2 & 0 & 0 & 1 & -1 & -1 & 0 & 0 & 0 & 0 & 0 & 0 & 0 & 0 & 0 & 0 & 0 & 0 & 0 & 0 & 0 & 0 & 0 & 0 & 0 & 0 \\
0 & 0 & -1 & 0 & 0 & 0 & 0 & 2 & 1 & 1 & 0 & 0 & 0 & 0 & 0 & 0 & 0 & 0 & 0 & 0 & 0 & 1 & 0 & 0 & 0 & -1 & -1 & 0 & 0 & 0 & 0 & 0 \\
0 & 0 & -1 & 0 & 0 & 0 & 0 & 1 & 2 & 1 & 0 & 0 & 0 & 1 & 0 & 0 & 0 & -1 & -1 & 0 & 0 & 0 & 0 & 0 & 0 & 0 & 0 & 0 & 0 & 0 & 0 & 0 \\
0 & 0 & -1 & 0 & 0 & 0 & 1 & 1 & 1 & 2 & -1 & -1 & 0 & 0 & 0 & 0 & 0 & 0 & 0 & 0 & 0 & 0 & 0 & 0 & 0 & 0 & 0 & 0 & 0 & 0 & 0 & 0 \\
0 & 0 & 0 & 0 & 0 & 0 & -1 & 0 & 0 & -1 & 2 & 1 & 0 & 0 & 0 & 0 & 0 & 0 & 0 & 0 & 0 & 0 & 0 & 0 & 1 & 0 & 1 & -1 & 0 & 0 & 0 & 0 \\
0 & 0 & 0 & 0 & 0 & 0 & -1 & 0 & 0 & -1 & 1 & 2 & 0 & 0 & 0 & 0 & 1 & 0 & 1 & -1 & 0 & 0 & 0 & 0 & 0 & 0 & 0 & 0 & 0 & 0 & 0 & 0 \\
0 & -1 & 0 & 0 & 0 & 0 & 0 & 0 & 0 & 0 & 0 & 0 & 2 & 1 & 1 & 0 & 0 & 0 & 0 & 0 & 1 & 0 & 0 & 0 & 0 & 0 & 0 & 0 & -1 & -1 & 0 & 0 \\
0 & -1 & 0 & 0 & 0 & 0 & 0 & 0 & 1 & 0 & 0 & 0 & 1 & 2 & 1 & 0 & 0 & -1 & -1 & 0 & 0 & 0 & 0 & 0 & 0 & 0 & 0 & 0 & 0 & 0 & 0 & 0 \\
0 & -1 & 0 & 0 & 0 & 1 & 0 & 0 & 0 & 0 & 0 & 0 & 1 & 1 & 2 & -1 & -1 & 0 & 0 & 0 & 0 & 0 & 0 & 0 & 0 & 0 & 0 & 0 & 0 & 0 & 0 & 0 \\
0 & 0 & 0 & 0 & 0 & -1 & 0 & 0 & 0 & 0 & 0 & 0 & 0 & 0 & -1 & 2 & 1 & 0 & 0 & 0 & 0 & 0 & 0 & 1 & 0 & 0 & 0 & 0 & 0 & 1 & -1 & 0 \\
0 & 0 & 0 & 0 & 0 & -1 & 0 & 0 & 0 & 0 & 0 & 1 & 0 & 0 & -1 & 1 & 2 & 0 & 1 & -1 & 0 & 0 & 0 & 0 & 0 & 0 & 0 & 0 & 0 & 0 & 0 & 0 \\
0 & 0 & 0 & 0 & 0 & 0 & 0 & 0 & -1 & 0 & 0 & 0 & 0 & -1 & 0 & 0 & 0 & 2 & 1 & 0 & 0 & 0 & 0 & 0 & 0 & 1 & 0 & 0 & 1 & 0 & 0 & -1 \\
0 & 0 & 0 & 0 & 0 & 0 & 0 & 0 & -1 & 0 & 0 & 1 & 0 & -1 & 0 & 0 & 1 & 1 & 2 & -1 & 0 & 0 & 0 & 0 & 0 & 0 & 0 & 0 & 0 & 0 & 0 & 0 \\
0 & 0 & 0 & 0 & 0 & 0 & 0 & 0 & 0 & 0 & 0 & -1 & 0 & 0 & 0 & 0 & -1 & 0 & -1 & 2 & 0 & 0 & 0 & 0 & 0 & 0 & 0 & 1 & 0 & 0 & 1 & 1 \\
-1 & 0 & 0 & 0 & 0 & 0 & 0 & 0 & 0 & 0 & 0 & 0 & 1 & 0 & 0 & 0 & 0 & 0 & 0 & 0 & 2 & 1 & 1 & 0 & 0 & 0 & 0 & 0 & -1 & -1 & 0 & 0 \\
-1 & 0 & 0 & 0 & 0 & 0 & 0 & 1 & 0 & 0 & 0 & 0 & 0 & 0 & 0 & 0 & 0 & 0 & 0 & 0 & 1 & 2 & 1 & 0 & 0 & -1 & -1 & 0 & 0 & 0 & 0 & 0 \\
-1 & 0 & 0 & 0 & 1 & 0 & 0 & 0 & 0 & 0 & 0 & 0 & 0 & 0 & 0 & 0 & 0 & 0 & 0 & 0 & 1 & 1 & 2 & -1 & -1 & 0 & 0 & 0 & 0 & 0 & 0 & 0 \\
0 & 0 & 0 & 0 & -1 & 0 & 0 & 0 & 0 & 0 & 0 & 0 & 0 & 0 & 0 & 1 & 0 & 0 & 0 & 0 & 0 & 0 & -1 & 2 & 1 & 0 & 0 & 0 & 0 & 1 & -1 & 0 \\
0 & 0 & 0 & 0 & -1 & 0 & 0 & 0 & 0 & 0 & 1 & 0 & 0 & 0 & 0 & 0 & 0 & 0 & 0 & 0 & 0 & 0 & -1 & 1 & 2 & 0 & 1 & -1 & 0 & 0 & 0 & 0 \\
0 & 0 & 0 & 0 & 0 & 0 & 0 & -1 & 0 & 0 & 0 & 0 & 0 & 0 & 0 & 0 & 0 & 1 & 0 & 0 & 0 & -1 & 0 & 0 & 0 & 2 & 1 & 0 & 1 & 0 & 0 & -1 \\
0 & 0 & 0 & 0 & 0 & 0 & 0 & -1 & 0 & 0 & 1 & 0 & 0 & 0 & 0 & 0 & 0 & 0 & 0 & 0 & 0 & -1 & 0 & 0 & 1 & 1 & 2 & -1 & 0 & 0 & 0 & 0 \\
0 & 0 & 0 & 0 & 0 & 0 & 0 & 0 & 0 & 0 & -1 & 0 & 0 & 0 & 0 & 0 & 0 & 0 & 0 & 1 & 0 & 0 & 0 & 0 & -1 & 0 & -1 & 2 & 0 & 0 & 1 & 1 \\
0 & 0 & 0 & 0 & 0 & 0 & 0 & 0 & 0 & 0 & 0 & 0 & -1 & 0 & 0 & 0 & 0 & 1 & 0 & 0 & -1 & 0 & 0 & 0 & 0 & 1 & 0 & 0 & 2 & 1 & 0 & -1 \\
0 & 0 & 0 & 0 & 0 & 0 & 0 & 0 & 0 & 0 & 0 & 0 & -1 & 0 & 0 & 1 & 0 & 0 & 0 & 0 & -1 & 0 & 0 & 1 & 0 & 0 & 0 & 0 & 1 & 2 & -1 & 0 \\
0 & 0 & 0 & 0 & 0 & 0 & 0 & 0 & 0 & 0 & 0 & 0 & 0 & 0 & 0 & -1 & 0 & 0 & 0 & 1 & 0 & 0 & 0 & -1 & 0 & 0 & 0 & 1 & 0 & -1 & 2 & 1 \\
0 & 0 & 0 & 0 & 0 & 0 & 0 & 0 & 0 & 0 & 0 & 0 & 0 & 0 & 0 & 0 & 0 & -1 & 0 & 1 & 0 & 0 & 0 & 0 & 0 & -1 & 0 & 1 & -1 & 0 & 1 & 2
\end{bmatrix}. \tag{170}$$

Its spectrum is $\{0^{(17)}, 2^{(4)}, 4^{(6)}, 6^{(4)}, 8^{(1)}\}$ of (71), and the edge operator is $M_1 = L_1 + I$, whose edge spectrum gives the string tension through the colour flux b_s.

Acknowledgments

Anthropic's Claude (Opus versions 4.6–4.8) was used for computational combinatorics/algebraic derivations, Python scripting, and manuscript editing carried out interactively, and PocketCAS for iOS and NetworkX with NumPy in Google Colab to independently verify the matrix calculations. Theoretical direction was provided by the author.

References

[1] M. Van Raamsdonk, *Building up spacetime with quantum entanglement*, Gen. Rel. Grav. **42**, 2323 (2010).

[2] T. Faulkner, M. Guica, T. Hartman, R. C. Myers, M. Van Raamsdonk, *Gravitation from entanglement in holographic CFTs*, JHEP **03**, 051 (2014).

[3] S. Ryu, T. Takayanagi, *Holographic derivation of entanglement entropy from the anti–de Sitter space/conformal field theory correspondence*, Phys. Rev. Lett. **96**, 181602 (2006).
[4] B. Swingle, *Entanglement renormalization and holography*, Phys. Rev. D **86**, 065007 (2012).
[5] C. Furey, $SU(3)_C \times SU(2)_L \times U(1)_Y (\times U(1)_X)$ *as a symmetry of division algebraic ladder operators*, Eur. Phys. J. C **78**, 375 (2018).
[6] A. Connes and J. Lott, *Particle models and noncommutative geometry*, Nucl. Phys. B Proc. Suppl. **18B**, 29 (1991).
[7] A. H. Chamseddine and A. Connes, *The spectral action principle*, Commun. Math. Phys. **186**, 731 (1997).
[8] T. P. Singh, *Towards deriving the Standard Model coupled to gravity from generalized trace dynamics via the spectral action principle*, Universe **12**(7), 205 (2026), doi:10.3390/universe12070205.
[9] J. D. Bekenstein, *Black holes and entropy*, Phys. Rev. D **7**, 2333 (1973).
[10] S. W. Hawking, *Particle creation by black holes*, Commun. Math. Phys. **43**, 199 (1975).
[11] A. D. Sakharov, *Vacuum quantum fluctuations in curved space and the theory of gravitation*, Sov. Phys. Dokl. **12**, 1040 (1968) [Dokl. Akad. Nauk SSSR **177**, 70 (1967)].
[12] H. Umegaki, *Conditional expectation in an operator algebra IV (entropy and information)*, Kōdai Math. Sem. Rep. **14**, 59 (1962).
[13] S. Navas *et al.* (Particle Data Group), *Review of Particle Physics*, Phys. Rev. D **110**, 030001 (2024).
[14] D. Buttazzo, G. Degrassi, P. P. Giardino, G. F. Giudice, F. Sala, A. Salvio, A. Strumia, *Investigating the near-criticality of the Higgs boson*, JHEP **12** (2013) 089, arXiv:1307.3536.
[15] G. Vidal, *Entanglement renormalization*, Phys. Rev. Lett. **99**, 220405 (2007), arXiv:cond-mat/0512165.
[16] G. Evenbly and G. Vidal, *Algorithms for entanglement renormalization*, Phys. Rev. B **79**, 144108 (2009), arXiv:0707.1454.
[17] A. E. Brouwer and W. H. Haemers, *Spectra of Graphs* (Springer, New York, 2012). Freely available at `https://homepages.cwi.nl/~aeb/math/ipm/ipm.pdf`.
[18] K. G. Wilson, *Confinement of quarks*, Phys. Rev. D **10**, 2445 (1974).
[19] J. Kogut and L. Susskind, *Hamiltonian formulation of Wilson's lattice gauge theories*, Phys. Rev. D **11**, 395 (1975).
[20] M. Visser, *Sakharov's induced gravity: a modern perspective*, Mod. Phys. Lett. A **17**, 977 (2002), arXiv:gr-qc/0204062.
[21] T. Jacobson, *Thermodynamics of spacetime: the Einstein equation of state*, Phys. Rev. Lett. **75**, 1260 (1995).
[22] E. Verlinde, *On the origin of gravity and the laws of Newton*, JHEP **04** (2011) 029, arXiv:1001.0785.
[23] N. D. Birrell and P. C. W. Davies, *Quantum Fields in Curved Space* (Cambridge University Press, 1982).
[24] I. L. Buchbinder, S. D. Odintsov, I. L. Shapiro, *Effective Action in Quantum Gravity* (IOP Publishing, Bristol, 1992).
[25] B. S. DeWitt, *The Global Approach to Quantum Field Theory*, Vols. I, II (Oxford University Press, 2003).
[26] A. Anderson, B. Holdom, *A comment on induced gravity*, Phys. Lett. B **141**, 339 (1984).
[27] M. Chaichian, M. Oksanen, A. Tureanu, *Sakharov's induced gravity and the Poincaré gauge theory*, in *Memorial Volume for Jacob Bekenstein* (World Scientific, 2019), arXiv:1805.03148.
[28] F. R. Klinkhamer, *Newton's gravitational coupling constant from a quantum of area*, Mod. Phys. Lett. A **26**, 1301 (2011), arXiv:1101.5370.
[29] A. Rényi, *On measures of entropy and information*, Proc. 4th Berkeley Symp. Math. Stat. Prob. **1**, 547 (1961).
[30] A. Lewkowycz, J. Maldacena, *Generalized gravitational entropy*, JHEP **08** (2013) 090.
[31] J. Szangolies, *The Standard Model symmetry and qubit entanglement*, Entropy **27**(6), 569 (2025).
[32] S. Weinberg, *A model of leptons*, Phys. Rev. Lett. **19**, 1264 (1967).
[33] S. L. Glashow, *Partial-symmetries of weak interactions*, Nucl. Phys. **22**, 579 (1961).
[34] A. Salam, *Weak and electromagnetic interactions*, in *Elementary Particle Theory*, ed. N. Svartholm (Almqvist & Wiksell, Stockholm, 1968), p. 367.
[35] A. M. Badalian and B. L. G. Bakker, *The radial Regge trajectories and leptonic widths of the isovector mesons*, arXiv:1603.04725 (2016).